© 2014 Olaoluwa Olufemi Adeniba

DEVELOPMENT OF HIGH-Q MICROMECHANICAL CELL MASS SENSOR (OPTIMIZING PARAMETERS FOR IN-PLANE MASS SENSORS)

BY

OLAOLUWA OLUFEMI ADENIBA

THESIS

Submitted in partial fulfillment of the requirements
for the degree of Master of Science in Mechanical Engineering
in the Graduate College of the
University of Illinois at Urbana-Champaign, 2014

Urbana, Illinois

Adviser:

Professor Rashid Bashir

Abstract

There exists a strong correlation between the behavior of a cell, its physical properties, and its surrounding environment. Biomechanics has led to an improved understanding of the way diseases evolve and their progression cycle, providing methods targeted towards curing these diseases.

Moreover, many studies have been carried out on the progression that occur to cell biophysics. More particularly, these studies on the mechanics of individual cells have pointed to their coordination and cycle, which helps us understand cellular metabolic and physiological process better. Development of more precise, versatile and reliable measurement tools and techniques will provide a greater understanding of cellular behavior and biophysical properties. Micromechanical systems (MEMS) technology can provide these tools – for analyzing single cells and give important and useful information about their biophysical properties.

In modern research, the ability to reliably investigate and understand these cellular properties requires measurement devices that provide high sensitivity, high throughput, and adaptability to include multiple on-chip functionalities. Many MEMS-based resonant sensors have been extensively studied and used as biological and chemical sensors. However, previous works have shown that there are several technology limitations that inhibit application of various mass sensors to mass measurement and analysis, including insufficient cell capture efficiency, media perfusion for long term growth, cell adhesion and cell movement/spreading.

The primary objective of this work is to theoretically characterize and compare the characteristics of resonant sensors vibrating in-plane (lateral mode) and out-of-plane (transversal) and note the

improvement when the microcantilever is excited in the in-plane direction. Our current out-of-plane resonant sensor while more effective than regular micro cantilevers, are less efficient as a sensing platform due to an additional liquid resistance exerted by the surrounding liquid. This work highlights the design of a relatively high-Q (quality factor) laterally vibrating mass sensor. It includes a review of other sensor geometries iteratively considered. A theoretical analysis and modelling of our optimal in-plane mass sensors are carried out.

Acknowledgements

I would like to acknowledge the inspirational guidance of my advisor, Dr. Rashid Bashir, your persistent drive and kind advice has helped a great deal. Thank you for your patience. Your excellent spirit is rare.

I appreciate Dr. Ilesanmi Adesida for his continued help and support. I would also like to thank Dr. Elise Corbin for being there to provide all the valuable resource. Special thanks to Kathy Smith for her sincere and heartfelt advice through thick and thin. Thanks to my friends and family for their encouragement through every tough time, I could never have finished my thesis without their selfless love and support!

Table of Content

List of Tables

List of Figures

Chapter 1

Introduction

Recent insights in the fields of cell cycle regulation and cancer would each have provided prime examples of research at the 'Frontiers of Science'. However, some of the most revealing information about both topics has been derived from the intersection of the two fields. The intent of this chapter is to introduce the basics of cells; cell cycle, cancer and their overlap. It has been established that cell cycle machinery controls cell proliferation and cancer is a disease of inappropriate cell proliferation. Understanding the molecular mechanisms of the deregulation of cell cycle progression in cancer can provide important insights into how normal cells become tumorigenic.

1.1 Cancer

Cancer is a complicated disease that stems from several mutations in a cell. These occurrence often affects and controls cell growth, and results in numerous biophysical properties. Cancer cells grow and divide at an unregulated, quickened pace and are able to invade other tissues. Cancer is not just one disease but many diseases. Its types can be grouped into broader categories. The main categories include:

- **Carcinoma** - cancer that begins in the skin or in tissues that line or cover internal organs
- **Sarcoma** - cancer that begins in bone, cartilage, fat, muscle, blood vessels, or other connective or supportive tissues.
- **Leukemia** - cancer that starts in blood-forming tissue such as the bone marrow and causes large numbers of abnormal blood cells to be produced and enter the blood.
- **Lymphoma and myeloma** - cancers that begin in the cells of the immune system.
- **Central nervous system cancers** - cancers that begin in the tissues of the brain and spinal cord.

As cancer spreads it makes it even harder to treat, and the survival rate decreases dramatically. It is therefore better diagnosed early while a greater understanding of cellular properties will aid in the future of cancer diagnoses. Among other causes of death, cancer ranks second in the United States of America (USA), and is becoming more widespread with 1.52 million new diagnoses made in 2010 alone [1]. Figure 1.1 depicts the causes of death in the USA.

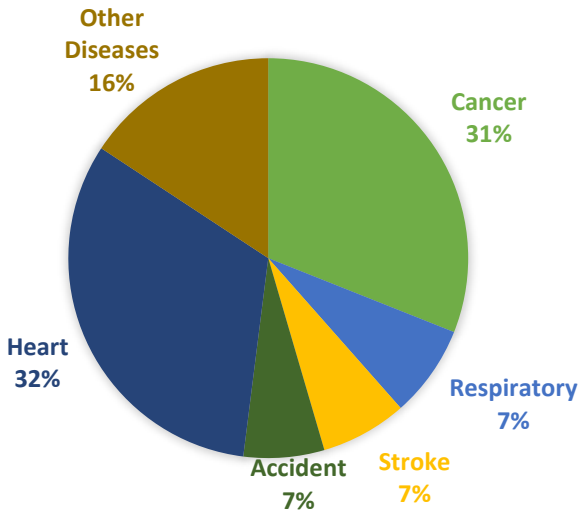

Figure 1.1 Causes of Death in the USA, Cancer ranks second. [Data from [16]]

1.2 Cell Biomechanics

1.2.1 Cell Architecture

Cells can be subdivided into the following subcategories:

1. Prokaryotes: Prokaryotes are relatively small cells surrounded by the plasma membrane, with a characteristic cell wall that may differ in composition depending on the particular organism. Prokaryotes lack a nucleus (although they do have circular or linear DNA) and other membrane-bound organelles (though they do contain ribosomes).

2. Eukaryotes: Eukaryotic cells are also surrounded by the plasma membrane, but on the other hand, they have distinct nuclei bound by a nuclear membrane or envelope. Eukaryotic cells also contain membrane-bound organelles, such as (mitochondria, chloroplasts, lysosomes, rough and smooth

endoplasmic reticulum, vacuoles). In addition, they possess organized chromosomes which store genetic material. [17]. Human cells, are eukaryotic. They are far more complex involving a more well-defined internal structure with multiple sub-cellular components, including separate membrane bound nucleus and organelles, seen in Figure 1.2 (b). The nucleus is a major component containing the chromosomes and DNA that drive major metabolic activity such as gene transcription and replication.

Growth and progression through the cell cycle is regulated by the nucleus. The cytoskeleton, which is the material structure of the cell acts as a cellular scaffolding to prevent the plasma membrane from collapsing to its lowest energy system. Its functionality includes cellular locomotion, cell-cell linkages, and cell-ECM linkages. The cytoskeleton is made up of three major types of filaments: actin microfilaments, microtubules, and intermediate filaments that play a significant role in the mechanical properties of a cell. Substrate stiffness and other environmental factors affect the cell structure, and in turn changing the functionality of the cell.

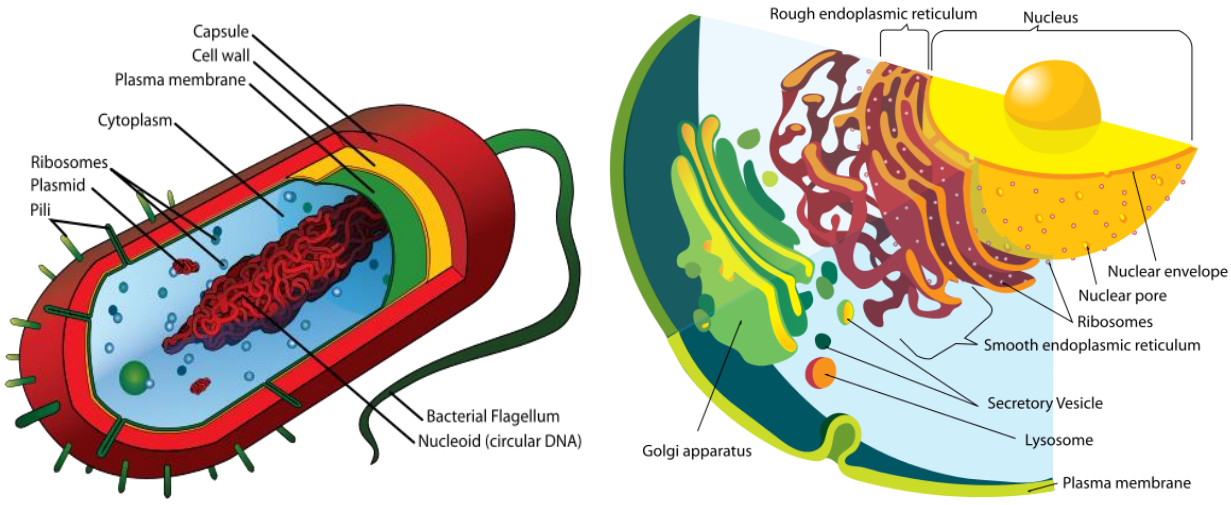

Figure 1.2: Schematic **Left**: prokaryotic, **Right**: eukaryotic cell cross-section showing the membrane bound organelles [Image from [17]]

1.2.2 Mechanical Properties of Cells

Biological matter often behaves both as an elastic solid and as a viscous fluid, and is therefore considered to be viscoelastic. Living cells and tissues, in spite of great biological complexity, can be characterized as viscoelastic matter. Cells behave in an elastic manner over short time scales in order to withstand sudden forces from surrounding cells, while over longer time scales they behave in a viscous manner. This property allows cells, for example, to squeeze inside narrow blood vessels or between other cells by undergoing large deformations in response to forces applied over long time scales.

Cellular viscoelasticity arises due to the co-existence of solid and liquid phases. Cells and tissues have high water content as well as a structural matrix consisting of polymers. These biopolymers, can support cell shape and provide cells with a structural rigidity. However, they are also highly dynamic and can undergo large scale rearrangements. A living cell is a complex dynamical system, which constantly undergoes remodeling to adapt to changing environmental conditions. Cells adapt their mechanical properties in order to match that of their surroundings. The mechanical changes in cells under normal conditions and in response to external forces may be highly complex and difficult to measure. However, recent advances in rheological techniques have enabled the measurement of the mechanical properties of living matter. Cellular mechanical properties can be measured by several advanced techniques such as Atomic Force Microscopy, compression between parallel plates, magnetic tweezers, optical cell stretching, flow cytometers and micro-cantilevers.

The mechanical properties of cells and their surroundings are important for regulating many biological functions such as cell growth, cell movement, wound healing, cancer metastases and cell differentiation or the determination of cell fate. In a landmark experiment a few years ago, it was discovered that stem cells (cells that have not specialized into particular types) grown on soft matrices differentiate into

different cell types depending on the elastic material of the matrix. For example, stem cells grown on soft surfaces with low values of elastic modulus become brain cells, while cells grown on stiff surfaces with high elastic modulus become bone cells. These findings showed that cellular biochemical and genetic response are linked to the physical properties of cells and their surroundings [18].

1.2.3 Cell Cycle and Cancer

Cancer is frequently considered to be disease of the cell cycle. Cancer cells differ from normal cells in many important characteristics. These includes the loss of differentiation, self-sufficiency in growth signals, limitless replicative potential, increased invasiveness, and decreased drug sensitivity (Hanahan and Weinberg, 2000). These differences do not arise simply from uncontrolled cellular growth, but rather from a cellular evolution. The increased incidence of cancer as a function of age has long been interpreted to suggest the progressive acquisition of mutations and epigenetic abnormalities in the expression of multiple genes that have diverse functions are required for tumorigenesis. An important group of these genes is involved in cell cycle checkpoints, which are positions of control that ensure the order of events in the cell cycle, and that integrate DNA repair with cell cycle progression.

Cell cycle transition is an ordered, tightly-regulated process that involves multiple checkpoints that assess extracellular growth signals, cell size, and DNA integrity. The somatic cell cycle is divided into four distinct phases (Fig. 1.3). During two of these phases, the cells execute the basic events in cell division like generation of a single and faithful copy of its genetic material (synthetic or S phase) and partitioning of all the cellular components between the two identical daughter cells (mitosis or M phase). The two other phases of cell cycle represent gap periods (G1 and G2), during which the cells prepare themselves for the successful completion of the S and M phases, respectively. When the cells cease proliferation, due either to specific antimitogenic signals or to the absence of proper mitogenic signaling,

then they exit the cycle and enter a non-dividing, quiescent state, known as G0. In addition, the cell cycle may be arrested at the G1 or G2 checkpoints that assess cell size, extracellular growth signals, and DNA integrity [19].

Related to these events are four factors that appear to control the entry into the M-phase:

1. The accumulation of a specific cellular mass is a factor for somatic cells. This is called the *mass factor*. Some cells need to obtain a specific growth rate for mitosis to begin. This is called the *growth rate factor*.
2. The time between successive M-phases appears to be controlled by timer or oscillator genes. This is the *time factor* and appears to be a factor in embryo cells.
3. The entry into the M-phase also requires completion of the S-phase. This insures that daughter cells receive complete DNA complements and is called the completion of chromosomal *replication factor*.

The process of replicating DNA and dividing a cell can be described as a series of coordinated events that compose a ‘‘cell division cycle,’’ illustrated for mammalian cells in Figure 1.3 (see legend for details). In this, at least two types of cell cycle control mechanisms are recognized: a cascade of protein phosphorylation that relay a cell from one stage to the next and a set of checkpoints that monitor completion of critical events and delay progression to the next stage if necessary [20].

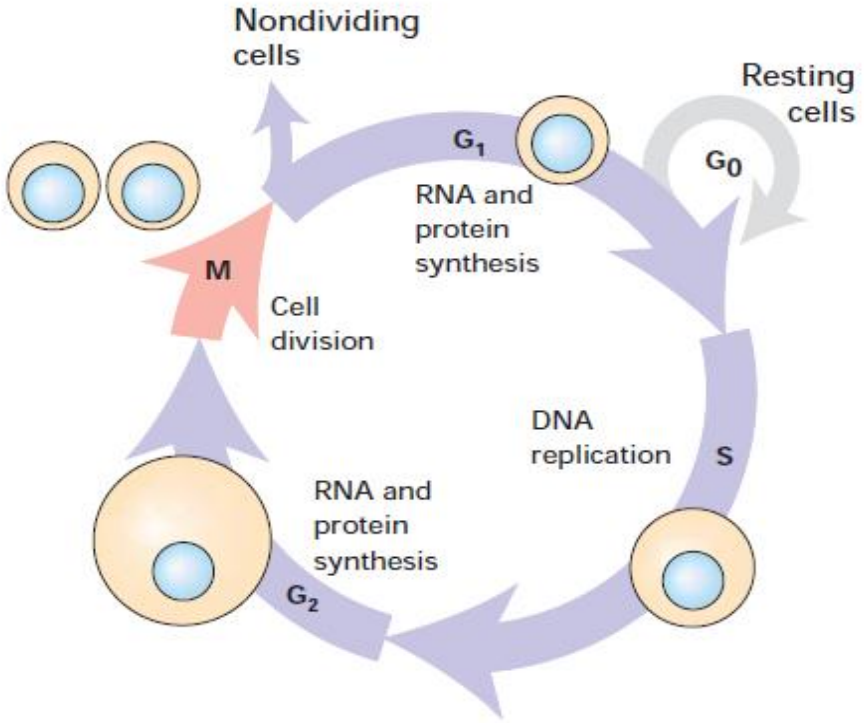

Figure 1.3: The mammalian cell cycle. In each cell division cycle, chromosomes are replicated once (DNA synthesis or S-phase) and segregated to create two genetically identical daughter cells (mitosis or M-phase). These events are spaced by intervals of growth reorganization (gap phases G_1 and G_2). Cells can stop cycling after division, entering a state of quiescence (G_0). Commitment to traverse an entire cycle is made in late G_1. Progress through the cycle is accomplished in part by the regulated activity of numerous CDK-cyclin complexes.[20]

The first type of control involves a highly regulated kinase family. A second type of cell regulation, checkpoint control is more supervisory. It is not an essential part of the cycle progression machinery. Cell cycle checkpoints sense flaws in critical events such as DNA replication and chromosome segregation. When checkpoints are activated, for example by underreplicated or damaged DNA, signals are relayed to the cell cycle-progression machinery. These signals cause a delay in cycle progression machinery, until the danger of mutation has been averted. Because checkpoint function is not required in every cell cycle, the extent of checkpoint function is no as obvious as that of components integral to the process, such as CDKs- Cyclin dependent Kinases.

Superficially, the connection between the cell cycle and cancer is obvious: cell cycle machinery controls

cell proliferation, and cancer is a disease of inappropriate cell proliferation. Fundamentally, all cancers permit the existence of too many cells. However, this cell number excess is linked in a vicious cycle with a reduction in sensitivity to signals that normally tell a cell to adhere, differentiate, or die. This combination of altered properties increases the difficulty of deciphering which changes are primarily responsible for causing cancer [20].

Chapter 2

Cell Micromechanics: Background, Properties and Methods

Mass and stiffness, and other biophysical properties are fundamental physiological properties that are regulated by environmental and genetic factors, which have implications in cell biology, tissue engineering, and the research of cancers and diseases. In some recent studies, it was shown that cell growth rate is a function of cell mass [2]. The cell mass homeostasis ensures that the cell mass and cell cycle transitions are coordinately linked [19]. This chapter provides a background on cell mass, growth rate and the current techniques used in measuring of these biophysical properties of cells. Some of the limitations of these technique are highlighted.

2.1 Cell Mass and Growth Rate

Cell growth is the process of building mass to increase size. A relevant study of interest in this field is the highlighting of factors that regulates overall cell growth and coordination of growth with cell cycle progression. A cell must maintain homeostasis, or equilibrium state, over the cell cycle to function properly. This is the regulation of the internal system of the cell for proper function. Many diseases occur as a result of an imbalance of cell size homeostasis, which is linked to the coordination of the cell cycle. Growth is a normal part of life; however, growth rate is dependent on species. Although there is significant variation between individuals, the internal workings and organs of a person are proportional to the body. As organisms grow their size is maintained. In an experiment [2], some individual cells were grown on a mass sensor and measured their mass for 50 hours. The results demonstrate that adherent human colon epithelial cells have increased growth rates with a larger cell mass, and the average growth rate increases linearly with the cell mass, at 3.25%/hr.

As explained in figure 1.2, the cell cycle is the period of time for cellular reproduction, including growth of the parent cell and its division into two daughter cells. Two distinct phases divide the cell cycle: interphase, the time period where the cell grows and acquires mass, and mitosis, the process where the cell divides. Interphase itself comprises three distinct segments: a gap, G1, where the cell grows in size, synthesis where DNA is replicated, and another gap, G2, for additional cell growth. Checkpoints exist after each gap to ensure the cell is prepared to enter either synthesis or mitosis.

2.2 Growth Models

There are two major models used to analyze the cell cycle: one based on an exponential increase and another based on a linear increase. Variations in growth rate over the cell cycle may elucidate mechanisms underlying cell growth better than the magnitude of growth rate alone.

Exponential growth rate for an individual cell is proportional to cell size mass, volume, or density during the cell cycle. Linear growth rate for an individual cell is constant meaning the cell increases size by the same amount regardless of its current size or state. The exponential growth rate is derived from the increasing amount of ribosomal machinery present in the cell that doubles along with size during the cell cycle. Since growth is dependent on the ribosomes, larger cells grow faster through more protein synthesis. However, cells should be in balanced growth where the bulk properties of cells remain unchanged for several generations, thus requiring additional cell size control mechanisms for cell size homeostasis over generations. If larger cells grow more rapidly than smaller ones, as in the exponential model, cell size variation in the population would increase in each generation. Because this does not occur, we know that if growth is exponential or, more generally, if it increases with cell size some mechanism must limit size variation in cells. In Mitchison.et.al [8], two approaches to understanding growth during the cell cycle are single-cell studies, where growth during the cell cycle of a single cell is

measured, and cell-culture studies, where growth during the cell cycle of a large number of cells as an aggregate is analyzed. Mitchison has proposed that single-cell studies, because they show variations in cell growth patterns, are more suitable for understanding cell growth during the cell cycle, and should be preferred over culture studies. Specifically, Mitchison argues that one can glean the cellular growth pattern by microscopically observing single cells during the division cycle. In contrast to Mitchison's viewpoint, it is argued here that the biological laws underlying cell growth are not to be found in single-cell studies. The cellular growth law can and should be understood by studying cells as an aggregate.

These ideas are applied to the controversy between proponents of linear growth as a possible growth pattern during the cell cycle and the proponents of exponential growth during the cell cycle. Differential (pulse) and integral (single cell) experiments are compared with regard to cell cycle analysis and it is concluded that pulse-labeling approaches are preferred over microscopic examination of cell growth for distinguishing between linear and exponential growth patterns. Even more to the point, aggregate experiments are to be preferred to single-cell studies.

The logical consistency of exponential growth – integrating and accounting for biochemistry, cell biology, and rigorous experimental analysis – leads to the conclusion that proposals of linear growth are the result of experimental perturbations and measurement limitations. It is proposed by Mitchison that the universal pattern of cell growth during the cell cycle is exponential.

2.2.1 Bulk Analysis Limitations

Populations of cells or bulk dynamics can produce to misleading results especially when measuring time dependent measurements. Early growth studies that could only study populations of cells have established a baseline for modern analysis techniques. Cellular heterogeneity within a population is a fundamental principle of cell biology, and should be a key consideration when investigating cells. However, as advanced tools are developed and we are able to capture growth on the single cell level, we

need to rethink our analysis to reflect our new capabilities. There has been several work that focussed on the understanding and analysis of individual cells and growth data and a review of single cell data using new techniques to determine cell growth rate on a cell-by-cell basis.

2.2.2 Volumetric Analysis Coulter Counter

One of the most popular methods that has been readily adopted in measuring the size or volume of a cell using methods such as a Coulter counter. Cell growth has been an on- going area of investigation. Coulter counters use the conductivity of a cell to measure the resistance change of the fluid as cells are directed between two electrodes. The change in resistance is recorded; this signal is directly proportional to the volume of the cell. [10]

Another method for volumetric calculations is flow cytometry. As a cell passes through a laser beam, it scatters light. The light scattered in the forward direction is referred to as the FSC parameter. This parameter is equivalent to the volume in a spherical cell. [11]

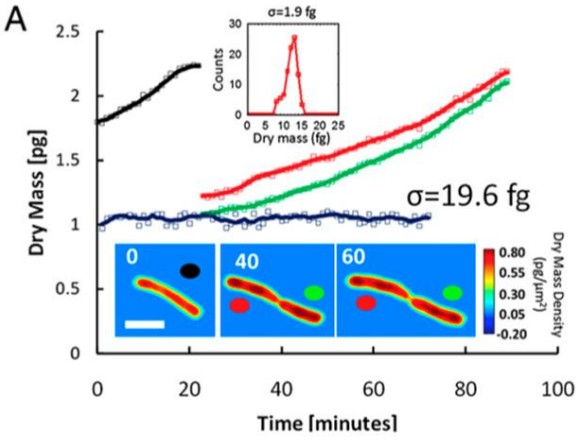

Figure 2.1: Spatial light interference microscopy (SLIM) estimates growth of E.coli with an integral[32]

The advancement of improved optics has led to the development of spatial light interference microscopy (SLIM). SLIM is able to measure the cell dry mass of a variety of adherent cells under many different conditions of time, size of measurement area, and cell type. When SLIM is combined with fluorescence imaging, it allows monitoring of single cell growth in each phase of the cell cycle. The total dry mass is calculated by performing an integral of an image of the data, indicating that this is another volume calculation based on optics. An example of these measurements can be seen in Figure 2.1 [19]

Although these methods are an appealing option for measuring cell growth, volume is not the sole measure of cell size. During cell growth, the components of a cell (proteins, nucleic acids, cytoplasm, etc.) are continuously changing with a constant flux of material; therefore volume is not the complete picture of the cell growth and the cell cycle. Thus, cell mass could be a better indicator of growth because it takes into account the changes in cellular composition, such as protein synthesis.

2.3 Cell Mass Sensing Methods

Microcantilevers are one of the most common forms of resonant sensors. They were first developed for atomic force microscopy (AFM) in 1986, but they have been used for many different types of measurements, including chemical and biological sensing. Fast response time, high sensitivity, and scalability are some of its advantages.

Since cantilevers are the simplest form of a resonant sensor, it also has a simple geometry it makes it easy to determine the effective spring constant. When mass is placed on the free end of a cantilever, the resonant frequency will shift. The resonant frequency of the cantilever is inversely proportional to the square root of the mass. The mass of the cells attached to the cantilever can be directly calculated from the resonance frequency of the cantilever. Scaling of the cantilever is an extremely desirable trait for easy

manipulation of the sensitivity based on the object's size and mass. This has made them a very attractive solution for various applications such as the detection of DNA, viruses, bacteria, spores, etc. One limitation of the system is the non-uniform mass sensitivity over the cantilever surface. This means that the mass reading is directly linked to the position of the cell on the cantilever and must be taken into account.

Microcantileves were first developed for atomic force microscopy (AFM), but have been used for many different types of measurements, everything from chemical and biological sensing. This is an especially attractive option due to fast response time, high sensitivity, and ability to array to upscale.

Microcantilevers are easy to fabricate, in a cleanroom facility. They allow for label-free, non-invasive long-term sensing of cells over long periods of time. This is ideal for studying growth curves of cells. The measurement equipment can be automated to take readings every few minutes to get good temporal resolution. There are many different ways to measure the cell mass, add in examples here of coulter counter, SLIM, other optical methods. Additionally, cantilevers have been used in various applications such as the detection of DNA, viruses, bacteria, spores, etc. [3].

The resonant frequency of the cantilever is inversely proportional to the square root of the mass, so, the mass of the cells attached to the cantilever can be directly calculated from the resonance frequency of the cantilever. One downside to this setup is the non-uniform mass sensitivity over the cantilever surface. This means that the mass reading is directly linked to the position of the cell on the cantilever and must be taken into account.

Dynamics of Cantilever Biosensors:

We represent a cantilever as a lumped model with mass, spring and damper system:

$$m^* \frac{d^2z}{dt} + c\frac{dz}{dt} + kz = \mathrm{F}e^{\mathrm{i}\omega t} \quad (2.1)$$

Where m is the mass, c is the damping coefficient, k is the spring constant, F is the force, and ω is the angular frequency. The resonant frequency of the system is described by Equation 2.1

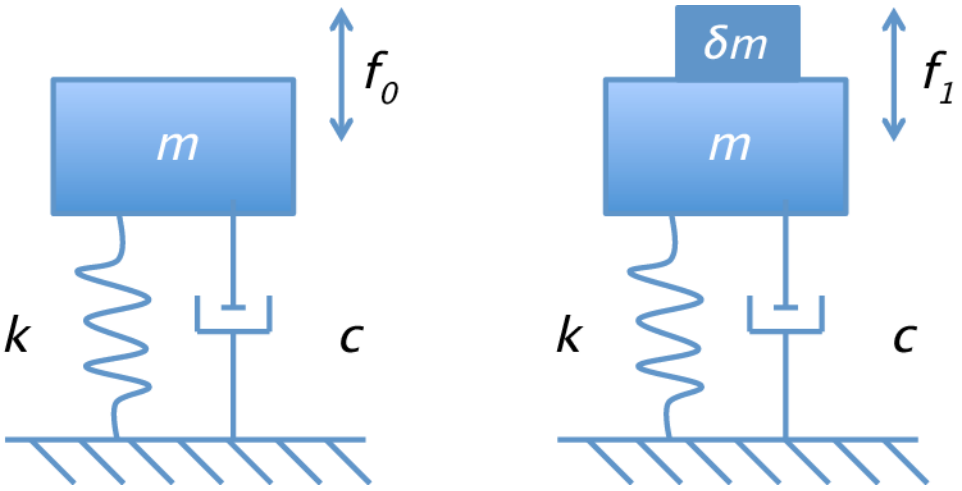

Figure 2.2: It is assumed that δm is a point mass on m and that the measurement is being taken in air, so the effect of damping, c, is very minimal. Unloaded (left) and loaded (right) resonant frequency diagrams. [2]

$$\text{Unloaded Resonant Frequency: } f_0 = \frac{1}{2\pi}\sqrt{\frac{k}{m}} \quad (2.2)$$

Where f_0 is the resonant frequency, k is the spring constant and m is the mass of cantilever.[2] From

Equation 2.2, Equation 2.3 takes into account the additional point mass from Equation 2.2, as shown in Figure 3.

$$\text{Loaded Resonant Frequency: } f_1 = \frac{1}{2\pi}\sqrt{\frac{k}{m+\delta m}} \tag{2.3}$$

Where f_1 the loaded resonant frequency, k is the spring constant, and m+δm is the mass of the cantilever plus a change in mass. The change in mass (δm) is modeled as a point mass [3]. Combining Equations 2.2 and 2.3 and rearranging terms, Equation 2.4 describes the change in mass.

$$\delta m = \frac{k}{4\pi^2}\left(\frac{1}{f_1^2} - \frac{1}{f_0^2}\right) \tag{2. 4}$$

Where δm is the change in mass, f_1 is the loaded resonant frequency and f_0 is the unloaded resonant frequency.

Presented in the sections below are methods that help in collecting cell mass information based on resonant behavior and data provided by the devices.

2.3.1 Cantilever Structure Array

This technique provides information about single, adherent cells. The cantilever array is a multiplexed iteration in silicon (Figure 2.3) of the basic cantilever design described in the previous section. The array allows for more cells to be measured at one time. Similar to the basic cantilever design, the cantilever arrays are faced with the same challenges as the basic cantilever design. They experience non-uniform mass sensitivity over the surface of the sensor.

This method is great because it takes the idea of a cantilever sensor and allows it to be multiplexed and run many different cell measurements in the same experiment.

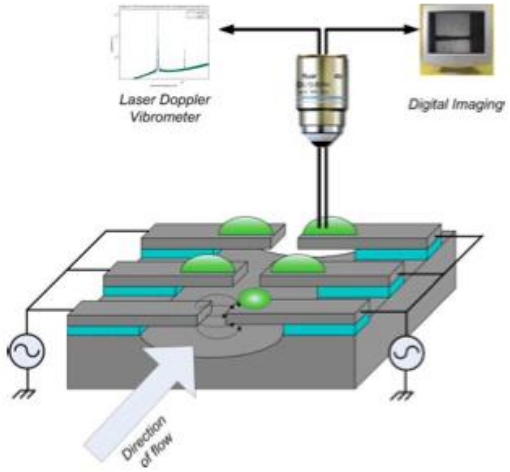

Figure 2.3: Cantilever Arrays [3]

One of the unique aspects of cantilevers is that they can be scaled up to arrays for high throughput. The small size of the cantilever allows for high sensitivity. They are a favorable method for non-invasively monitoring the mass of a single cell. These cantilever arrays are used to measure adherent cell mass. They consist of many silicon cantilevers arranged in parallel for the measurement of adherent cells.

As mentioned above, one downside to this method is the sensitivity dependence of the cell location on the cantilever. As the cell gets closer to the tip of the cantilever, the measurement gets more accurate. This is cumbersome and requires a lot many of calculations to overcome. Additionally, the sensors are highly damped when in a liquid environment, further decreasing the sensitivity. This damping can be overcome, however, by placing the liquid environment inside of the cantilever as demonstrated in the next method.

2.3.2 Hollow Cantilever Structure

The hollow cantilever structures consist of a silicon cantilever with an embedded microfluidic channel. It cleverly decreases the effects of damping in liquid seen in the cantilever array sensors by creating a microfluidic channel inside the cantilever (Figure 2.4) and then performing the measurements in a vacuum environment. This reduction in damping allows mass to be measured with femtogram precision. These structures are used to measure the single cell mass of suspended cells.

This method is great because it cleverly decreases the effects of damping in liquid seen in the cantilever array sensors by creating a microfluidic channel inside the cantilever and then performing the measurements in a vacuum environment. Also, the dependence on the cell's location does not matter, since the cell is not adhered to the cantilever surface.

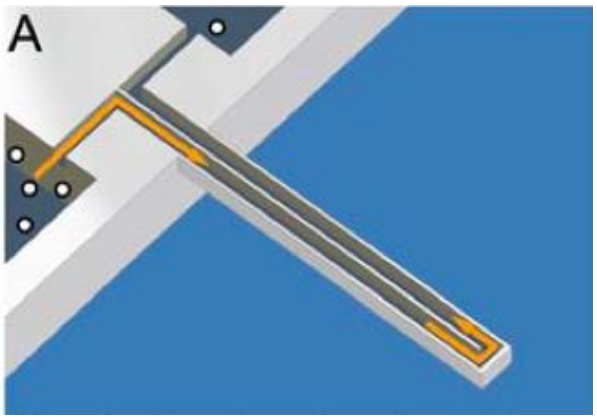

Figure 2.4: Suspended Microchannel Resonator (SMR) [19]

Bryan et. al. in 2009 called the hollow cantilever design a suspended microchannel resonator (SMR) when it was used to measure mass, density and volume of yeast throughout the cell cycle. The device oscillates at a frequency proportional to its mass, like the general cantilever equation, but the mass of this cantilever changes as a cell is repeatedly flowed back and forth through the microfluidic chamber,

creating a dynamic trap that allows for consecutive buoyant mass measurements of the same cell. [19] Unfortunately, this method is only valid for cells that thrive in a suspended culture. Most cells, however, are adherent and grow best when they are attached to a surface similar in stiffness to their native tissue extracellular matrix.

This suspended microchannel resonator (SMR) consists of a silicon cantilever with an embedded microfluidic channel that resonates at a frequency proportional to its mass, which changes as individual cells flow through the channel. The SMR measures mass with femtogram precision, allowing for rapid determination of the growth rate in a fraction of a complete cell cycle. The flow direction was continuously altered in the microfluidic channel to create a dynamic trap that allows for consecutive buoyant mass measurements of the same cell. Unfortunately, this setup does not allow for mass measurements of adherent cells because the cells must be constantly be flowed back and forth through the channel. This setup does provide very little damping, therefore very high mass sensitivity. The device is used in a vacuum and the fluid is located inside the cantilever. [2]

While this method provides excellent sensitivity, it requires the cells to be in suspension, which is not the best environment to study adherent cells. Adherent cells grow and behave most normally when then can adhere to a surface similar in stiffness to their native tissue environment.

2.3.3 In-plane Mode: Quartz Crystal Microbalances

Gryte, et. al. in 1993 first used the Quartz Crystal Microbalances to monitor the attachment and detachment of anchored mammalian cells in real time. It (the QCM) consists of an AT-cut piezoelectriz quartz crystal in between two electrodes. It functions by applying an alternating voltage potential across the quartz crystal by the two excitation electrodes on opposite sides of the quartz crystal. This causes the

crystal to oscillate at a characteristic resonant frequency. [31]

An advantage it offers is that the QCM allows the monitoring of adherent cells, unlike the hollow cantilevers, and the sensitivity of the measurement is not dependent on the location of the cell, unlike the traditional cantilever design. The benefit of this method when it was first developed was real-time measurements. They used this technique to study lysis and detachment of Vero cells in real-time. Previous adhesion studies were tedious and the interpretation of the data was up to the user, very subjective.

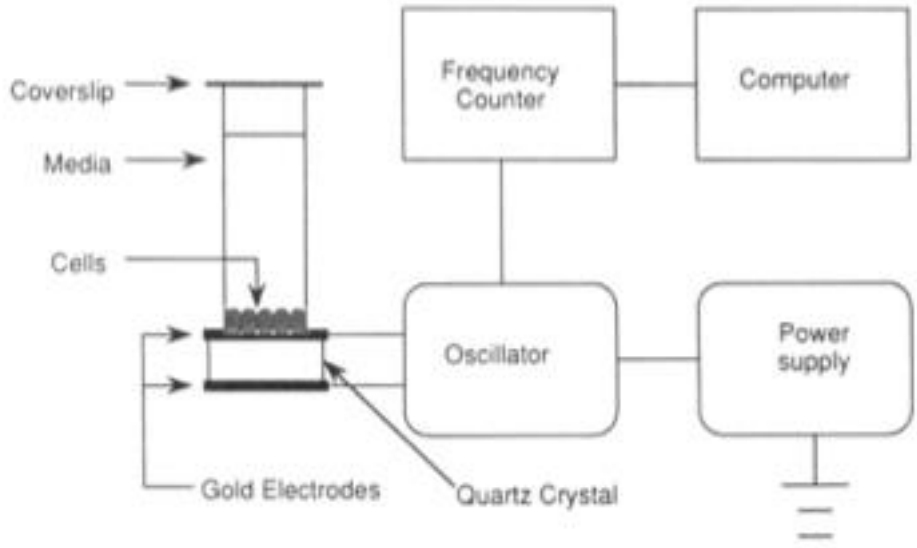

Figure 2.5: Setup of Quartz Crystal Microbalance (QCM) [12]

The QCM is controlled by the following equation:

$$\Delta f = \frac{-2f_0^2 \Delta m}{A\sqrt{\rho_q \mu_q}} \tag{2.5}$$

Where Δf is the resonant frequency decrease, f is the intrinsic frequency of the crystal, Δm is the change in elastic mass (grams), A is the electrode area, ρ_q is the density of the quartz, and μ_q is the shear modulus.

This equation assumes rigid layer behavior, where the resonant QCM frequency depends on the mass, m, attached to the quartz crystal surface. This is called the Sauerbrey relationship.

The Sauerbrey relationship can be used to determine the change in mass at the surface of the quartz crystal. Any mass bound to the surface will oscillate with similar lateral displacement as the oscillating quartz crystal. If the body is very stiff, then no energy is lost and the oscillations are elastic. If the body is not stiff, then there is energy lost and the process is inelastic. The sensitivity of this 'quartz crystal nanobalance' is 0.1µg, but it is valid only for very small elastic masses. It does not function for masses larger than 2% of the crystal mass.

While this method is good at determining bulk, adherent cell information, it does not provide information about single cells. This leads us to the current resonant sensor explained in the next chapter.

Chapter 3

MEMS Resonant (Out-of-Plane) Pedestal Measurement

There are many existing techniques used to investigate the physical properties of cells on the micro scale. The ability to reliably investigate and understand these properties requires measurement devices that provide high sensitivity, high throughput, and adaptability to include multiple on-chip functionalities.

This chapter highlights the current use of micromechanical sensors to measure the properties including cell mass. It covers the review of principles behind the techniques employed and the measurement procedures. Firstly, Laser Doppler Vibrometer Test setup is considered after which, a review of the principles of cantilever resonant sensors for cell mass measurements, and then discuss the specific experimental process, some results and many important considerations for extracting mass from resonant frequency shift. Also, the resolution, sensitivity and quality factor are reviewed after which, the limitations of this measurement techniques discussed.

3.1 Design of Pedestal Sensors

The work presented in this section involves advances in MEMS technology to measure the biophysical properties of individual adherent cells. Being able to accurately measure the biophysical properties of cells will benefit efforts in cancer diagnosis and treatment, understanding cell-to-cell communication, and tissue engineering. Until very recently, microcantilevers are effectively used for mass sensing because of their potential for measurements with high sensitivity and high throughput.

However, it is obvious that cantilever beam structure has a non-uniform mass sensitivity and that calculation of mass depends strongly on placement of the object on the sensor. This constitutes a huge disadvantage in mass sensing of biological targets that must first be captured on the devices.

The difficulty of appropriate mass placement ultimately limits the accuracy of mass measurements made with the cantilever structure [1, 13]. To overcome this limitation, a MEMS resonant platform sensor has been designed to eliminate spatially dependent and non-uniform mass sensitivity [1], and can be used to measure the mass and long-term growth rate of single adherent cells. [7]

The sensor structure comprising the four-beam string and a pedestal was designed to minimize the variation of the displacement amplitude across the vibrating platform. The sensor is a square pedestal (60 × 60 μm2) suspended over a 50 μm pit by four beams acting as springs (l =80 μm, w = 4 μm). This unique structure, through both modeling and experimental data, exhibited a maximum 4% difference in mass sensitivity at any position on the pedestal.

In the case of measurement in liquid, it is challenging to determine the resonance frequency due to the high viscous damping and the resulting low quality factor. This constitutes a problem on its own since the sensor must remain in liquid.

Actuation in liquid also required a strong external force, and the sensor is actuated by passing an actuation current through the sensor in a static magnetic field to generate a Lorentz force [1, 14].

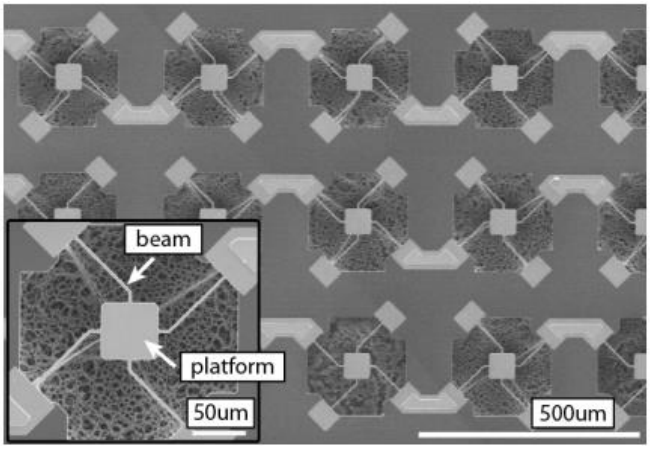

Figure 3.1: SEM image showing a sensor array; and an individual sensor is emphasized.

3.2 Laser Doppler Vibrometer Test Setup

The LDV is used to measure the vibration of the sensors. Its setup as shown in figure (3.2) includes a resonant pedestal sensor technology that hinges on a change in resonant frequency to calculate information about mass changes.

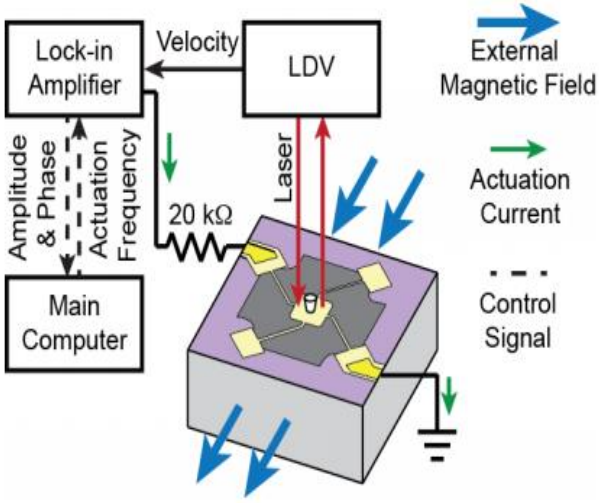

Figure 3.2- Overview of mass measurement with a sensor. The use of an electromagnetic actuation with a Laser Doppler vibrometer (LDV) system to measure the velocity of the vibrating platform

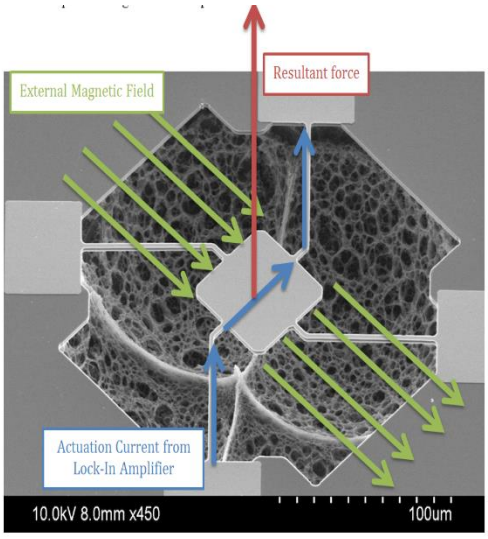

Fig 3.3: Diagram of chip showing the direction of Lorentz force [2]

The initial frequency is driven by Lorentz force as depicted in Figure 3.3 and (3.1) below:

$$\mathbf{F} = q(\mathbf{E} + \mathbf{v} \times \mathbf{B}) \qquad (3.1)$$

Figure 3.4 shows a laser Doppler vibrometer (LDV) system that reads the velocity of the vibrating MEMS sensor platform to ultimately determine the resonant frequency of the device. This happens in conjunction with a feedback system and a lock-in amplifier through monitoring the difference in phase between applied actuation current and sensor vibration.

The excitation frequency is updated based on this phase until it reaches the value of the resonant frequency. This procedure is used to estimate the resonant frequency of the devices in a series of different states to extract the mass of the adhered cell.

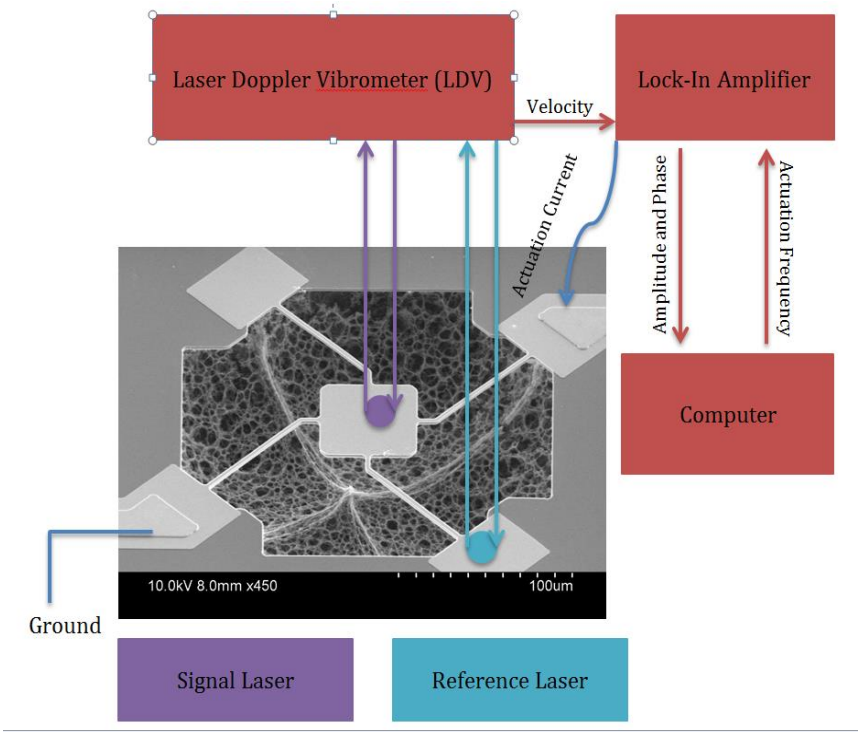

Figure 3.4 Schematic showing flow of signal and block diagram of Experimental Setup

3.2.1 Frequency shift operation

The shift in the resonant frequency is employed in measuring the mass of an object of interest attached to the sensor. This is because the resonant frequency of the device is inversely proportional to the square root of the total mass. Hence, the configuration of a cantilever helps in calculating its effective spring constant and device resonant frequency.

The procedure entails that the device is placed directly on the free end of the cantilever, then, the mass may be directly calculated from resonance frequency shift and the known spring constant of the device.

Figure (c) shows a shift in measured resonant frequency when mass is added. We can write the equation describing the deflection of the cantilever, z in terms of time, t. Note that here the cantilever is represented through a lumped model with a mass, m and subjected to a harmonic excitation force, $Fe^{i\omega t}$

We can therefore write the cantilever deflection, z in terms of time, t.

$$m^* \frac{d^2z}{dt} + c\frac{dz}{dt} + kz = Fe^{i\omega t} \qquad (3.2)$$

Where m* = 0.24m is the effective mass which accounts for the cantilever mass distribution; c is the damping coefficient; k is the spring constant; F is the amplitude of the excitation; and is the angular frequency of the excitation [13]. This system has a resonant frequency, f_0, which is described by equation 3.3

$$f_0 = \frac{1}{2\pi\omega 0} = \frac{1}{2\pi}\sqrt{\left(\frac{k}{m^*}\right)} \quad (3.3)$$

To calculate the change in mass, Δm from a resonant frequency shift Δf, we derive (3.4) from (3.3).

3.3 Cell Mass Measurement

For each sensor in the array, three different resonant frequencies are measured by the LDV as follows:

1. "Dry Frequency" Measurement: This entails the measurement of resonant frequency of each sensor in air, without the addition of any culture media or cell. It is used to extract the spring constant of each individual sensor and compensate for minute sensor-to-sensor differences that may exist from chip fabrication. The calculations are shown in Equations d below.

$$\omega = 2\pi f = \sqrt{\left(\frac{k}{m}\right)} \quad (3.4)$$

where ω is the angular frequency, f is the frequency, k is the spring constant, and m is the mass.

2. "Wet Frequency" Measurement: This entails the measurement of resonant frequency of each sensor in growth (culture) media after sterilizing and functionalizing the pedestal.
where k_{dry} is the spring constant in air, k_{wet} is the spring constant in liquid, m is the mass, and f is the frequency.

The "wet frequency measurement" provides a reference frequency that is necessary for running the cell mass measurement described next. During this measurement, the media contributes a damping effect to the chip. It also helps to infer the mass of each empty pedestal in the presence of culture media.

The dry or wet sensor can be modelled as a simple dynamic oscillator with the following governing equation.

$$K_{wet} = K_{dry} = m(2\pi f)^2 \quad (3.5)$$

$$m_{platform} = \frac{K_{wet}}{\left(2\pi f_{wet_{empty}}\right)^2} \quad (3.6)$$

where $m_{platform}$ is the mass of the empty pedestal that holds the cells, k_{wet} is the spring constant in liquid, $f_{wet,\ empty}$ is the frequency of an empty pedestal in liquid (reference frequency).

3. "Cell Mass" Measurement: This entails the measurement of resonant frequency of each sensor in growth (culture) media with cells on the pedestal surface.

The mass of the cell is calculated from the dry frequency and wet frequency measurements parameters. The equations e and f are used.

$$m_{cell+platform} = \frac{k_{wet}}{(2\pi f_{wet})^2} \quad (3.7)$$

where $m_{cell+platform}$ is the mass of a pedestal with a cell, k_{wet} is the spring constant in liquid, f_{wet} is the frequency of the pedestal with a cell in liquid.

Consequently, the mass of the cell can be extracted from the differences in masses (in media) with and without the cell as shown in equation (h) below:

$$m_{cell} = m_{cell+platform} - m_{platform} = \frac{k_{wet}}{4\pi^2}\left(\frac{1}{{f_{wet}}^2} - \frac{1}{{f_{wet\ empty}}^2}\right) \quad (3.8)$$

where m_{cell} is the mass of the cell on the pedestal, $m_{cell+platform}$ is the mass of a pedestal with a cell, $m_{platform}$ is the mass of the empty pedestal, k_{wet} is the spring constant in liquid, f_{wet} is the frequency of the pedestal with a cell in liquid, $f_{wet,\ empty}$ is the frequency of the empty pedestal. Figure 3.5 below shows a plot of the mass of a cell with again their various resonant frequencies discussed above.

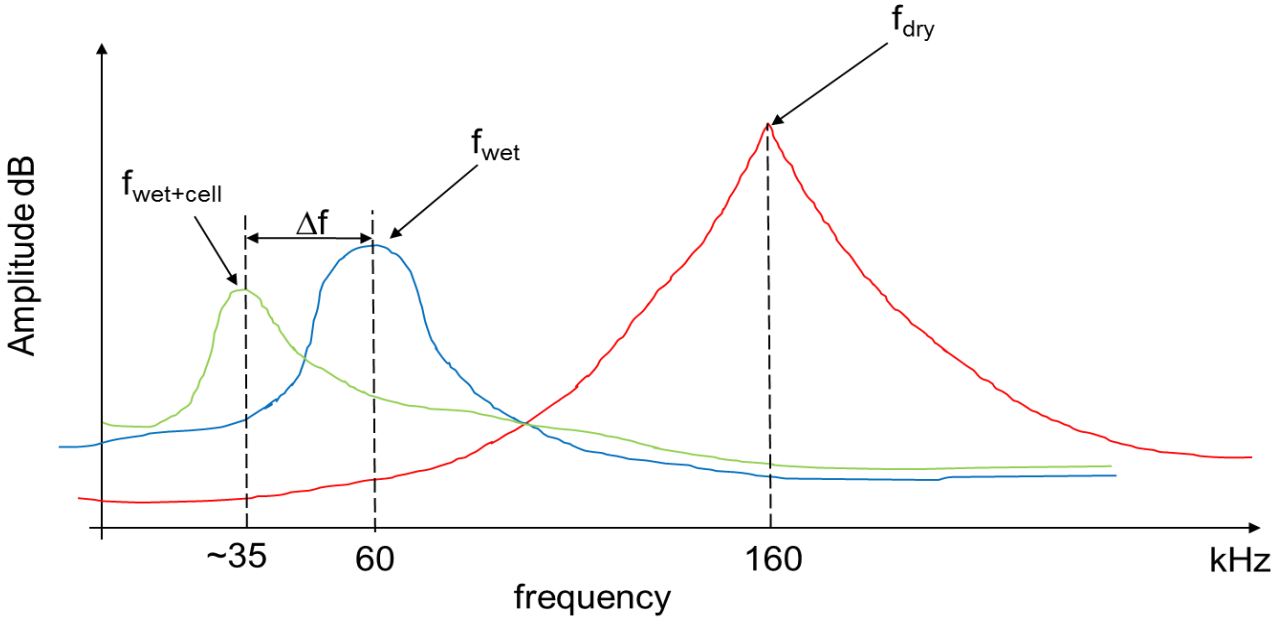

Figure 3.5: Frequency response of the sensor in air (red) in media without cell (blue) and in media with cell (green).

3.4 Sensor Material and Fabrication

Silicon-on-Insulator (SOI) wafers with a 2 µm device layer and a 0.3 µm buried oxide layer (BOX) were used as the starting material. A 25 nm silicon dioxide layer was grown by a thermal oxidation, to electrically insulate the device layer from the subsequent metal layers. The first lithographic process to define the first metal layer for electrode and sensor platform used S-1508 (AZ Electronic Materials) and LOR-3A (Microchem) for subsequent liftoff process. Then chrome (10 nm) and gold (50 nm) layers were deposited by e-beam evaporator and patterned by a liftoff process. The second lithographic process with AZ-9260 (AZ Electronic Materials) defined the etch mask for following silicon etching. The first metal layer and the photoresist layer from the second lithography were used to define the areas of sensor structure. Then, the exposed device layer was etched completely by ICP RIE to form the springs and the platform. A third photolithographic step with LOR-20B (Microchem) and AZ-9260 was used for the

second liftoff process, followed by the deposition of a 100-nmchrome layer and a 900-nmgold layer for wire-bonding pads. A release window was defined by the fourth lithograph process (AZ-9260) and the exposed BOXwas etched by RIE, leaving the silicon substrate exposed. Through the release window, the exposed Si substrate was etched by xenon difluoride (XeF2) to release the sensor structure to form a “pit” beneath the platform and springs. After XeF2 etching, the photoresist and the BOX were removed by buffered hydrofluoric acid (BHF) etching and solvent cleaning. A 100 nm thick silicon dioxide layer was deposited with plasma enhanced chemical vapor deposition (PECVD)
for insulation. The PECVD oxide on the bonding pads was selectively etched for wire-bonding with BHF. Finally, each die was attached to a printed circuit board and wire-bonded.

Through MEMS fabrication processes, a 9 × 9 array of 81 resonant mass sensors that achieves spatially uniform mass sensitivity was fabricated. Each sensor within the array consists of a square pedestal (60 × 60μm2) suspended by four beam springs (length = 80μm, width = 4μm, thickness = 2μm) over an approximately 50 μm deep pit. The 45º or half fold orientation of the beams as shown in figure a, b and c allows for high stress at their edges, ensuring that the dips keeps the mass sensitivity of the sensor or error due to cell position to be less than 4%. Conversely, if the beam had straight edges it causes steeper deeps and hence, making the potential cell positioning error larger. A 90º beam fold orientation would give the best vibrational performance except that is hard or almost impossible to fabricate.
The sensor operates in a first resonance mode, where the platform vibrates vertically at approximately 160 kHz in air and approximately 60 kHz in liquid. Our sensor shows mass sensitivity of 3 Hz/pg in air and 221 Hz/ng in liquid. [1]

Media / Parameters	**In Air**	**In Media**
Mass Sensitivity	3 Hz/pg	221 Hz/ng
Resonant Frequency	160kHz	60kHz
Quality factor	4.8	1.5

Table 3.1: Showing Sensitivity, Resonant frequency and quality factor values of resonant mass sensor in air and media

3.5 Limitation of out-of-plane resonant mass sensor:

Since a 9 × 9 array of 81 resonant mass sensors was fabricated, each sensor is traversed to measure the mass of cells on each sensor. In our experiment, the cell was cultured on the sensor array and the resonant frequencies and optical images of each selected sensor were collected every 30 to 40 minutes for over 60 hours. Hence, the individual cell growth rates are observed after an apparent change in mass. Meanwhile, the liquid surrounding the cell imposes a hydrodynamic loading that reduces the quality factor and resonant frequency of the sensor making the measurement noisy. For example, in our experiment, the resonant frequency in air is 160 kHz, while in liquid, it is 60kHz.

A better *temporal resolution* is therefore needed for a higher precision of measurement with time, and consequently, allowing for quicker observations of the rate of detachment of cells from the surface of these sensors. This leads to our proposed higher-Q factor design in the next chapter.

Chapter 4

Simulation & Design for Optimal In-Plane Mass Sensors

Many MEMS-based resonant sensor have been extensively studied and used as biological and chemical sensors. Our current out-of-plane resonant sensor while more effective than regular micro cantilevers, are less efficient as a sensing platform due to an additional liquid resistance exerted by the surrounding liquid. This chapter highlights the design of a relatively high Q-factor laterally vibrating mass sensor. It includes a review of several sensor geometries iteratively considered. It also covers the theoretical analysis and modelling of optimal in-plane sensor. The pedestal is modelled as a series of laterally vibrating euler-beams and a mass-spring damper system . The characteristics of laterally vibrating in air and viscous liquid media are theoretically evaluated. These characteristics include resonant frequency, quality factor, and mass sensitivity, which can be calculated from the frequency response of the pedestal's deflection.

4.1 Motivation and Introduction:

Generally speaking, MEMS-based sensors have various applications in electronics, photonics, mechanics, chemistry and biology, etc. Resonant sensors are characterized in many different ways by their sensitivity, resolution and selectivity. The sensitivity is the ratio of the magnitude of the output signal to the magnitude of the input quantity to be measured. The resolution is a measure of the minimum change of the input quantity to which the chemical sensor can respond, which is also called the limit of detection (LOD).

The selectivity is the degree to which the resonant sensor can distinguish one input quantity from another. Basically, a sensor with high sensitivity, low limit of detection, and high selectivity is desired.

For microcantilever-based MEMS resonant sensors, the two important characteristics are the resonance frequency and quality factor. The resonance frequency is the frequency of a vibrating system at which the response amplitude is a relative maximum. When operating at a resonant frequency, even a small periodic driving force can produce a large-amplitude vibration because the system can store and easily transfer energy between kinetic energy and potential energy. When the system reaches its steady state, the energy loss of the system is equal to the excitation energy from the driving forces in each cycle. Without driving forces, the amplitude of the system will reduce exponentially due to the energy loss. The quality factor is dependent on the damping mechanisms that are the sources of energy loss. It is a dimensionless parameter that describes how damped an oscillator or resonator is. Equivalently, the quality factor characterizes a resonator's bandwidth relative to its resonance frequency. Higher quality factor indicates a lower energy loss per cycle compared to the maximum stored energy of the system.

As discussed in chapter 3, for the current out-of-plane design, the resonant frequency of each selected sensor can be collected every 30 to 40 minutes for over 60 hours. This is because of the amount of pedestal that has to be traversed through the array and the speed at which the resonant frequency are measured. Essentially, the liquid surrounding the sensor imposes a hydrodynamic loading that reduces the quality factor and temporal resolution of the sensor which makes the measurement noisy and hard to take. In order to minimize the liquid resistance and improve its performance for mass sensing, the in-plane torsional mode of vibration is investigated. High sensitivity, portability, multiple target sensing, diverse applicability, and low cost are the good motivations for the design, development and synthesis of resonant microcantilever array sensors. Other areas of applications of these include the field of genomics, proteomics, food engineering and chemistry.

Surface stress (static mode) and mass change (dynamic mode) are important parameters of interest for micro cantilevers applied as a sensor. The focus of this chapter is on the dynamic mode. This is because

it is a challenging task to vibrate a microcantilever array in liquid environment. The operation requires efficient coupling of external excitation energy to the microcantilever avoiding anomalous additional acoustic frequencies originating from the liquid chamber. It also needs a bubble free fluid flow system, optimally focused parallel laser beams and sufficient laser power to pass through the air-liquid-air interface for optical detection of cantilever motion. In order to achieve resonance in the mechanical structure of a MEMS resonant sensor, the device must be excited by an actuator and set to resonate by varying the excitation frequency. The most popular and widely used excitation methods are capacitive actuation and piezoelectric actuation. In our analysis, we simulated a microcantilever in viscous liquid (media) through the use of an hydrodynamic function that represents a loading incurred by the liquid and backtracked the parameter like mass sensitivity, resonant frequency, quality factors based on some formulae provided.

4.2 In-Plane Mass Sensor

The mechanical structure in a MEMS-based sensor can operate in different modes. In general, the motion is described as either out-of-plane or in-plane with respect to the plane formed by the resonant sensor's two largest dimensions. Out – of – plane vibrations include transverse, also called bending or flexural, and torsional motion. In – plane vibrations include lateral also called in-plane bending, and longitudinal, also called extensional or axial motion. Several designs are considered after which we present the equation of motion for our optimal design. Among the different sensor platforms, in – plane resonant-based sensors are of high interest since they have high sensitivity and quality factor and supposedly, they can be easily fabricated.

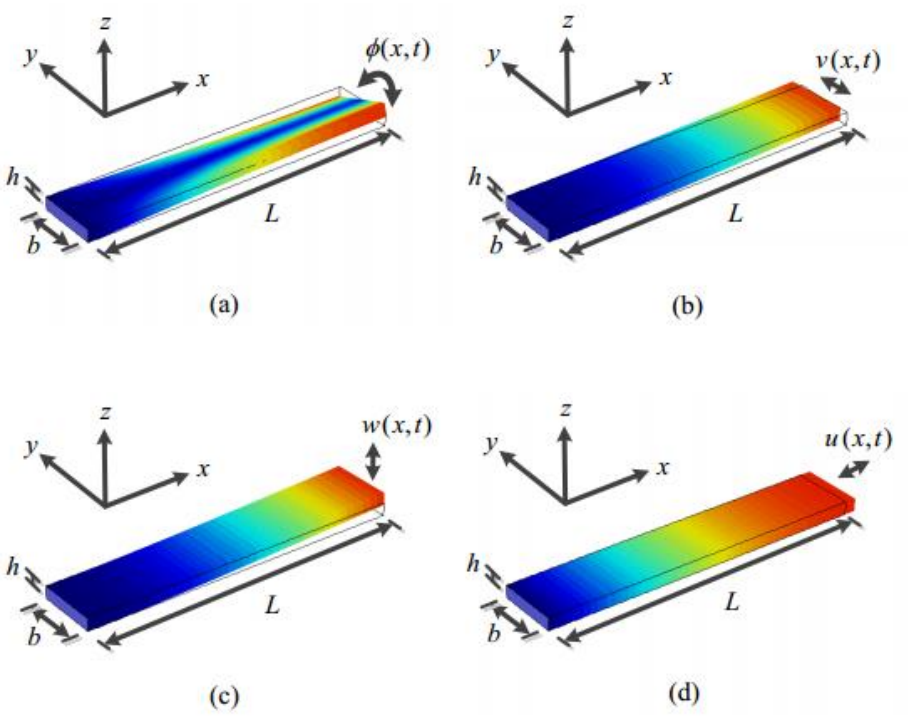

Figure 4.1: Geometry of a microcantilever (or beams) with length L, width b, and thickness h, vibrating (a) torsionally, (b) laterally, (c) transversely, (d) longitudinally, where ϕ, v, w, u are the rotational deflection (angle) in y-z plane, deflection in y direction, deflection in z direction, and deflection in x direction respectively. The color coding represents the deflection in the relevant direction[30]

4.2.1 Designs of In-Plane Resonant Sensor

In this section, several design types are considered, explored and analyzed. As described in Figure 4.1 (b) and (d) above, our sensor design entail some in – plane sensor, with lateral (in-plane bending) and longitudinal or extensional/axial vibrations.

Design 1:

This sensor consists of a square pedestal (60 × 60µm^2) suspended by two beam springs (l = 80µm, w = 4µm, thickness = 2).

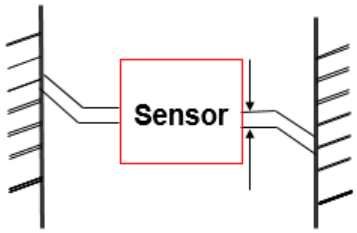

Figure 4.2: **Left:** Schematic showing sensor platform suspended by two beam springs (length = 80µm, width = 4µm, thickness = 2µm).

Design 2a:

This sensor consists of a rectangular pedestal (60 × 90µm^2) suspended by no beams.

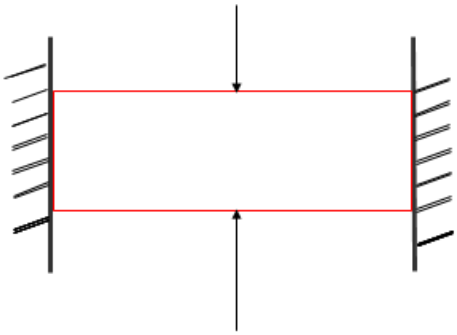

Figure 4.3 Sensor platform suspended by two beam springs (length = 80µm, width = 4µm, thickness = 2µm).

Design 1 and 2 can be modelled as a mass-spring damper below:

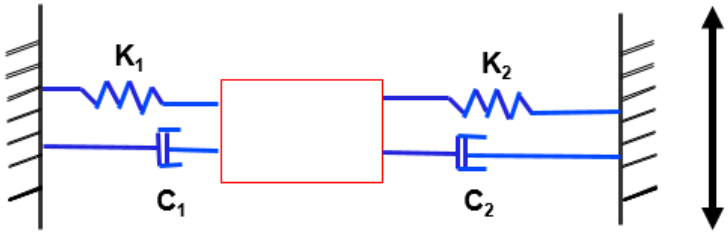

Figure 4.4: Schematic showing mass-spring model of designs 1 and 2. $K_{1,}$ K_{2}, representing spring constants of the beams (design 1) and fixed supports (design 2).

Design 2b

This sensor consists of a square pedestal (60 × 60µm^2) suspended by two beam springs (l = 80µm, w = 4µm, thickness = 2).

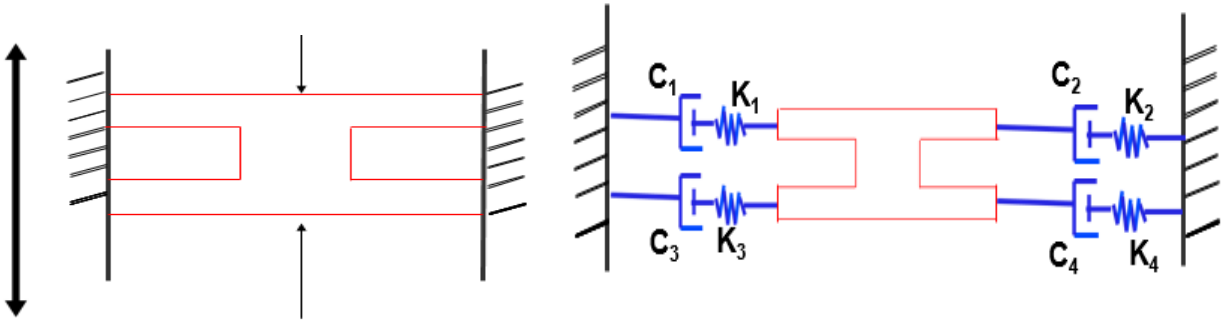

Figure 4.5: **Left:** Schematic showing doubly-clamped sensor suspended by four beam springs (length = 80µm, width = 4µm, thickness = 2µm). The arrow show the direction of vibration. **Right:** Mass-spring model of designs 3. $K_{1,}K_{2}, K_{3,}K_{4,}$ denote the spring constants of the beams, while, $C_{1,}C_{2}, C_{3,}C_{4,}$ denote their damping coefficients.

Design 3

This sensor consists of a circular pedestal ($60 \times 60\mu m^2$) supported by two elastic beams (length = 80µm, width = 4µm, thickness = 2 µm).

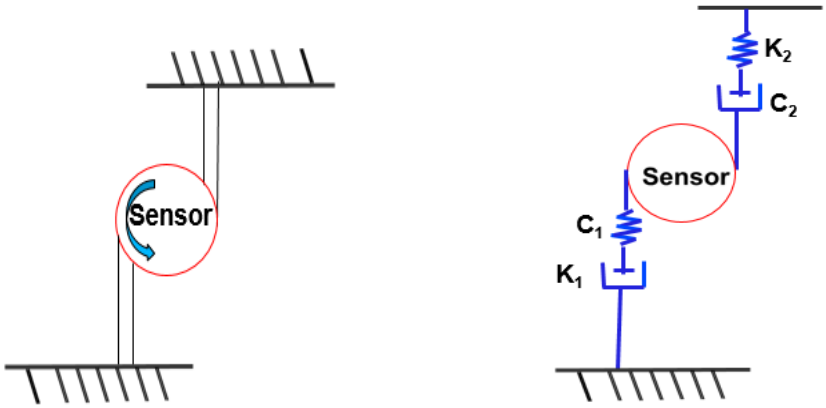

Figure 4.6: **Left:** 60µm-diameter circular sensor platform supported by two beams (length = 80µm, width = 4µm, thickness = 2µm) **Right:** Mass-spring model of designs 4. $K_{1,}K_2$ denote the spring constants of the beams, while, $C_{1,}C_2$, denote their damping coefficients

Design 4

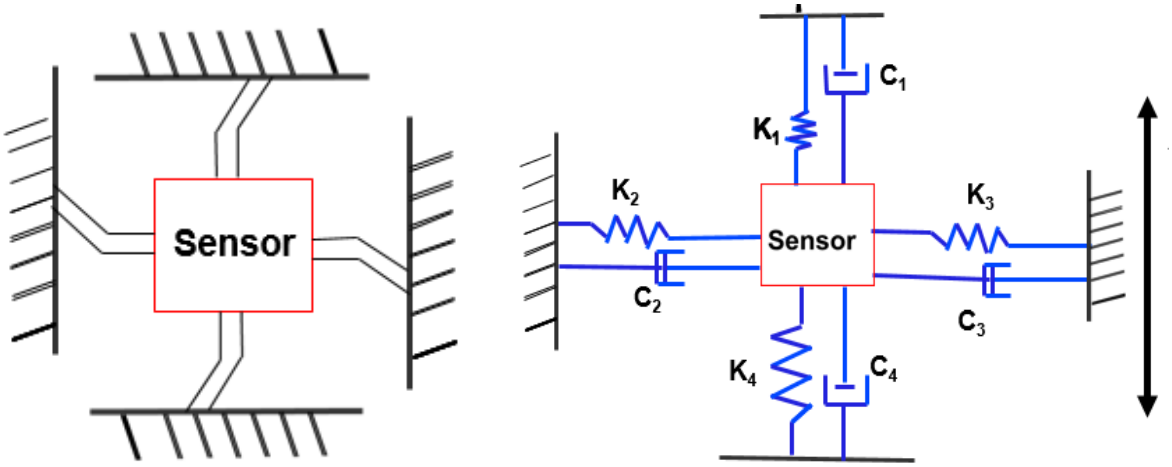

Figure 4.7 **Left:** Sensor platforms supported by four beams (length = 80µm, width = 4µm, thickness = 2µm) **Right:** Mass-spring model of design 5. K_1, K_2, K_3, K_4 denote the spring constants of the beams, while, C_1, C_2, C_3, C_4, denote their damping coefficients.

4.2.2 Theoretical Framework: Equation of Motion:

The various geometries can be modelled as:

a) A mass-spring-damper system
b) A series of laterally vibrating *Euler Beams*

(a) above will be used for determining our dry frequency response and (b) for wet frequency response (simulated in a viscous liquid medium) . The analysis of the various models are shown below:

4.2.2.1 Mass- Spring - Damper System:

The mass-spring damper systems used in modelling the resonant sensors presented above can be modelled using the Newtonian or Euler-Lagrange formulation, we consider the latter here:

$$\frac{d}{dt}\left(\frac{\partial L}{\partial \dot{q}_i}\right) - \left(\frac{\partial L}{\partial q_i}\right) + \frac{\partial P}{\partial \dot{q}_i} = Q_i \,, \tag{4.1}$$

where L is the lagragian, K$e - V$. Ke , V being the Kinetic and potential energy of the system. $\dot{q}_i$, the generalized coordinates, Q_i, the generalized external inputs and P, the power function, representing

In the equation above, i is the number of independent variables describing the motion of the system. Since, design 5 above is a generalization of all our designs, we will derive the equation of motion of our system and adapt it to other designs. We show design 5 in its dynamic mode below:

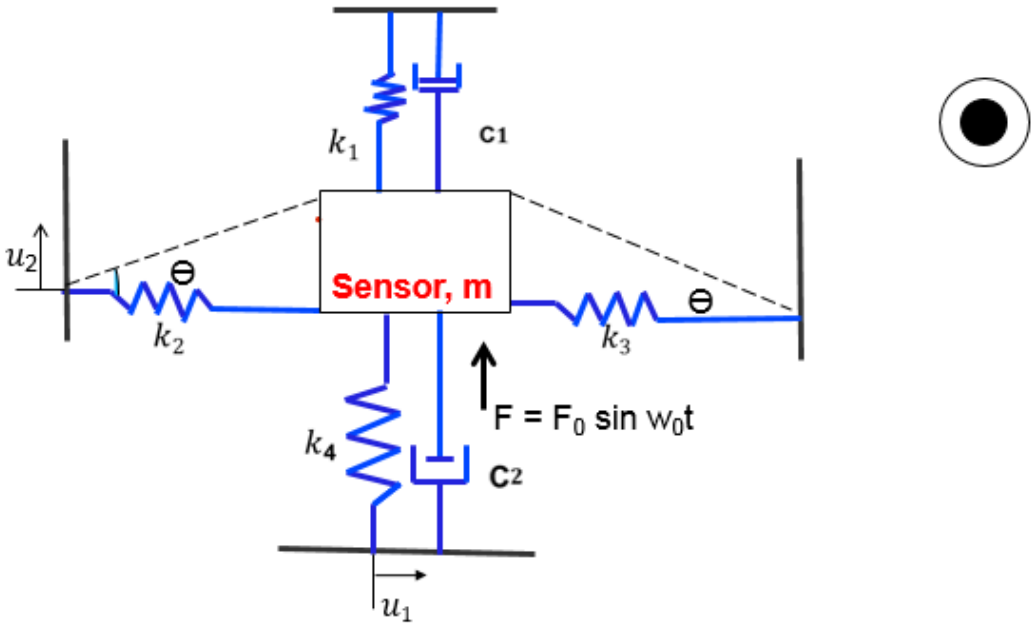

Figure 4.8**:** Mass-spring model of design 5. Schematic shows directionality of the sensor.

For design 5,

$$\mathrm{K}e = \frac{1}{2}m\dot{u}^2, \mathrm{V} = -\frac{1}{2}k_1u_1 + \frac{1}{2}k_4u_2 + \frac{1}{2}\frac{k_2}{Cos\,\theta}\,u_2 + \frac{1}{2}\frac{k_3}{Cos\,\theta}\,u_2\,, \tag{4.2}$$

$$Q_i = F_{,} \tag{4.3}$$

$$q = \begin{pmatrix} u_1 \\ u_2 \end{pmatrix}, \tag{4.4}$$

$$\mathrm{P} = -\frac{1}{2}C_1\dot{u}_1{}^2 + \frac{1}{2}C_2\dot{u}_2{}^2\,, \tag{4.5}$$

Applying the E-L, equation (4.1) then becomes:

$$m\ddot{u}_2 + (C_2 - C_1)\dot{u}_2 + \left(\frac{k_2 + k_3}{Cos\,\theta} - k_1 + k_4\right)u_2 = F \tag{4.6}$$

Design 5 above is a generalization of all other designs, hence, the frequency responses of all the designs are variants of design 5. This model will be used in determining the dry frequency response of our proposed system. The results are shown in the next chapter.

4.2.2.2 A Series of Laterally Vibrating Euler Beams

The Euler-Bernoulli beam theory is well established in such a way that engineers are very confident with the determination of stress field or deflections of the elastic beam based on this theory. Here, we express the system response in terms of inherent parameters, we model the design as an Euler beam:

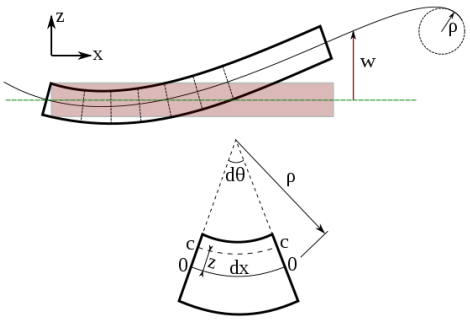

Figure 4.9: Bending of an Euler–Bernoulli beam. Each cross-section of the beam is at 90 degrees to the neutral axis. [Image from [26]]

The Euler–Bernoulli equation describes the relationship between the beam's deflection and the applied load [26]:

$$EI\frac{d^4w}{dx^4} = q(x), \tag{4.7}$$

Simulation results, shown in the next chapter are carried out in MATLAB. The geometry of a laterally excited microcantilever, with dimensions on the order of microns, is shown in Figure 4.11. It is generally assumed that L>>b, allowing for the application of Euler-Bernoulli beam theory. This assumption generally holds true for microcantilevers. The equation of motion for the laterally excited beam in a vacuum is given by:

$$EI_{lat}\ \frac{\partial^4 v(x,t)}{\partial x^4} + \rho_B bh\ \frac{\partial^4 v(x,t)}{\partial x^4} = F_y(x)e^{j(\omega lat)t}\ , \tag{4.8}$$

Where

$$I_{lat}\ = b^3h/12, \tag{4.9}$$

In (4.8), E is the Young's modulus, ρ_B is the mass density of the beam, $b\ and\ h$ represent the breadth and height of the cantilever. $F_y(x)$ is the position – dependent forcing function per unit length operating at an angular frequency of I_{lat} has the width cubed instead of the thickness (as is the case in traverse excitation) indicating that the flexural rigidity is larger for beams undergoing lateral vibration. When the microcantilever is operating in a viscous liquid medium, an additional force from the medium affects the microcantilever and the equation of motion is [24];

$$EI_{lat}\ \frac{\partial^4 v(x,t)}{\partial x^4} + \rho_B bh\ \frac{\partial^4 v(x,t)}{\partial x^4} = F_y(x)e^{j(\omega lat)t} + F_{medium,lat}\,(x,t), \tag{5.0}$$

The force per unit length, $F_{medium,lat}\,(x,t)$ is partially out-of-phase with the displacement, and can be represented as

$$F_{medium,lat}\,(x,t) = -g_{1,lat}\ \frac{\partial v(x,t)}{\partial t} - g_{2,lat}\ \frac{\partial^2 v(x,t)}{\partial t^2} \tag{5.1}$$

Where $-g_{1,lat}$ and $-g_{2,lat}$ are coefficients associated with the fluidic damping force per unit length and fluidic inertial force (displaced fluidic mass) per unit length respectively.

4.3 Design Considerations.

In the design of a resonant sensor, major considerations are given to characteristics including resonant frequency, quality factor, and mass sensitivity, which can be calculated with respect to the geometry of the resonant pedestal. We would use the following formulae in obtaining the characteristic values of our current in-plane and proposed out-of-plane sensors.

4.3.1 Resonant Frequency

The resonant frequency of a MEMS resonant sensors is a very important characteristic. This is the frequency of a vibrating system at which the response amplitude is a relative maximum. When operating at a resonant frequency, even a small periodic driving force can produce a large-amplitude vibration because the system can store and easily transfer energy between kinetic energy and potential energy. When the system reaches its steady state, the energy loss of the system is equal to the excitation energy from the driving forces in each cycle. Without driving forces, the amplitude of the system will reduce exponentially due to the energy loss. An analytic expression for the resonant frequency of a laterally vibrating microcantilever in viscious liquid has been obtained from the (5.0) as:

$$f_{res,lat} = \frac{\alpha_i^2}{2\pi}\sqrt{\frac{k_{lat}}{M_{lat}}}, \tag{5.1}$$

Where

$$k_{lat} = \frac{EI_{lat}}{L^3}, \tag{5.1a}$$

$$M_{lat} = \left(\rho bhL + Lg_{2,lat}\right) + \cdots$$

$$+ L\frac{\left(\left({}^{g_{1,lat}}/_{\omega_{res,lat}}\right) + \left(\frac{\omega_{lat}}{2}\right)\frac{d}{dw}\left({}^{g_{1,lat}}/_{\omega}\right)\right)}{\left({}^{m}/_{L} + g_{2,lat} + \left(\frac{\omega_{lat}}{2}\right)\frac{d}{dw}\left(g_{2,lat}\right)\right)}\left({}^{g_{1,lat}}/_{\omega}\right) \tag{5.1b}$$

And

$$g_{1,lat} = \frac{\pi}{4}\rho_L b^2 \Gamma_{lat,I}(Re, \frac{h}{b})\omega_{lat} \quad (5.1c)$$

$$g_{2,lat} = \frac{\pi}{4}\rho_L b^2 \Gamma_{lat,R}(Re, \frac{h}{b}) \quad (5.1d)$$

where α_i is the a constant dependent on the mode number ($\alpha_i \cong 1.875$ for the fundamental flexural mode). $\Gamma_{lat,R}$ and $\Gamma_{lat,I}$ are the real and imaginary parts of the hydrodynamic function, a normalized version of the hydrodynamic force (to be defined in the next section) that depends on the aspect ratio h/b and the Reynolds number (Re) of the medium. The Reynolds number is a measure of the ratio of inertial forces to the viscous forces acting on the beam, and is defined as:

$$Re = \frac{\rho_L \omega_{lat} b^2}{4\eta} \quad (5.2)$$

Where ρ_L and η are the mass density and dynamic viscosity of the fluid, respectively.

4.3.2 Quality Factor

The quality factor is dependent on the damping mechanisms that are the sources of energy loss. It is a dimensionless parameter that describes how damped an oscillator or resonator is. Equivalently, the quality factor characterizes a resonator's bandwidth relative to its resonance frequency. Higher quality factor indicates a lower energy loss per cycle compared to the maximum stored energy of the system.

With low loss, the quality factor can be approximated as [25]:

$$Q_{lat} = f_{res,lat}/\Delta f_{3dB} \quad (5.3)$$

Where Δf_{3dB}, is the 3-dB bandwidth of the system around resonance. With certain assumptions about $g_{1,lat}$ and $g_{2,lat}$. Quality factor can be found from the equation of motion as:

$$Q_{lat} = \left(2\left(1 - \sqrt{1 - \frac{g_{1,lat}/\omega_{lat}}{\rho_B bh}} \right) \right)^{-1} \quad (5.4)$$

4.3.3 Mass Sensitivity

The sensitivity is the ratio of the magnitude of the output signal to the magnitude of the input quantity to be measured. *Mass*- sensitivity, defines as the mass required to cause a unit change in frequency.

For a dynamic mode MEMS-based sensor, the mass sensitivity is the ratio of the magnitude of the resonance frequency shift to the magnitude of the mass change and is given as [25]:

$$Sm = \left| \frac{\Delta f_{r,i}}{\Delta M} \right|, \quad (5.5)$$

$f_{r,i}$ is the resonance frequency associated with the i-th vibration mode.

The analytical expression for the mass sensitivity of a laterally vibrating beam is [25];

$$S_m = \lambda_{m,lat} f_{res,lat} \quad (5.6)$$

Where,

$$\lambda_{m,lat} = \frac{\left(\left(g_{1,lat}/\omega_{lat} \right) + g_{1,lat}/\omega_{lat} + \left(\frac{\omega_{lat}}{2} \right) \frac{d}{dw} \left(g_{1,lat}/\omega \right) \right) L^2}{2M_{lat}\left(\rho bhL + Lg_{2,lat} + L\left(\frac{\omega_{lat}}{2} \right) \frac{d}{dw}\left(g_{2,lat} \right) \right)^2} - \frac{1}{2M_{lat}} \quad (5.7)$$

When the beam is operating in air or low viscosity media, the effective mass can be approximated as the beam mass, $Mlat \cong \rho BLbh$. Table 2 shows a comparison of both laterally (in-plane) and traversally (out-of-plane) vibrating beams of similar geometry in terms of some characteristics.

4.4 Hydrodynamic force function:

When a microcantilever is vibrating in an infinite viscous liquid medium (either in the in-plane or out-of-plane direction), the fluid acts to oppose the movement of the microcantilever, applying an opposing hydrodynamic force. However, this hydrodynamic force is not always applied perpendicularly to the surface of the microcantilever, as shown in Fig. 4.11

The hydrodynamic force can conceptually be decomposed into a force parallel with the surface of the beam (the shear or frictional force) and a force perpendicular to the surface of the beam (the pressure force). The hydrodynamic function is found to be [30];

$$\Gamma_{lat}\ (Re) = \frac{F^*_{medium,lat}}{j\pi n\ ReV_0 e^{j\omega t}} = \frac{2\sqrt{2}}{\pi\sqrt{Re}}(i+j) \qquad (5.8)$$

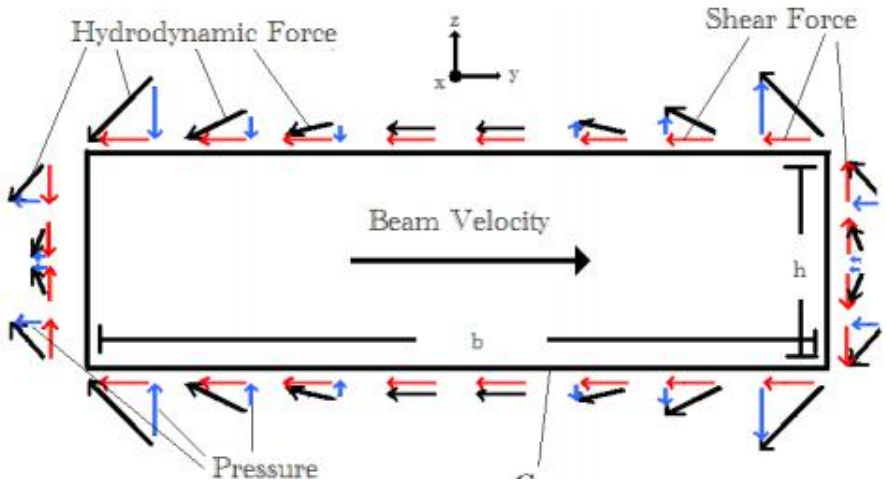

Figure 4.10 Hydrodynamic forces acting on the surfaces of a cross-section of a laterally vibrating microcantilever in fluid [Image from [24, 25]]

4.5. Comparison between Lateral (In – Plane) and Transversal (Out-of-Plane) Vibration

4.5.1 Resonant Frequency Ratio

$$\frac{f_{res,lat}}{f_{res,trans}} = \frac{b}{h}\sqrt{\frac{M_{trans}}{M_{lat}}}, \tag{5.8}$$

$$M_{lat} = \left(\rho bhL + Lg_{2,trans}\right) + \cdots$$

$$+ \frac{\left(\left({}^{g_{1,trans}}/_{\omega_{res,trans}}\right) + \left(\frac{\omega_{ltrans}}{2}\right)\frac{d}{dw}\left({}^{g_{1,trans}}/_{\omega}\right)\right)}{\left({}^{m}/_{L} + g_{2,trans} + \left(\frac{\omega_{trans}}{2}\right)\frac{d}{dw}\left(g_{2,trans}\right)\right)}\left({}^{g_{1,trans}}/_{\omega}\right) \tag{5.8a}$$

$g_{1,lat}$ and $g_{2,lat}$ are defined in 5.1 (c) and 5.1(d)

4.5.2 Quality Factor Ratio

$$\frac{Q_{lat}}{Q_{trans}} = \frac{\rho_B bhL + g_{2,lat}\,\Gamma_{1,lat}}{\rho_B bhL + g_{2,trans}\,\Gamma_{1,lat}} \tag{5.9}$$

$\Gamma_{1,lat}$ and $\Gamma_{1,lat}$ are defined in (5.8)

4.5.3 Mass Sensitivity Ratio

$$\frac{S_{m,lat}}{S_{m,trans}} = \frac{f_{res,lat}}{f_{res,trans}}\frac{M_{trans}}{M_{lat}} = \frac{b}{h}\left(\frac{M_{trans}}{M_{lat}}\right)^{3/2} \tag{5.10}$$

The ratios above are used in generating a comparison between our current out – of – plane (transversal) system and proposed in-plane (lateral) resonant sensor in viscous media (glycerol is used here).

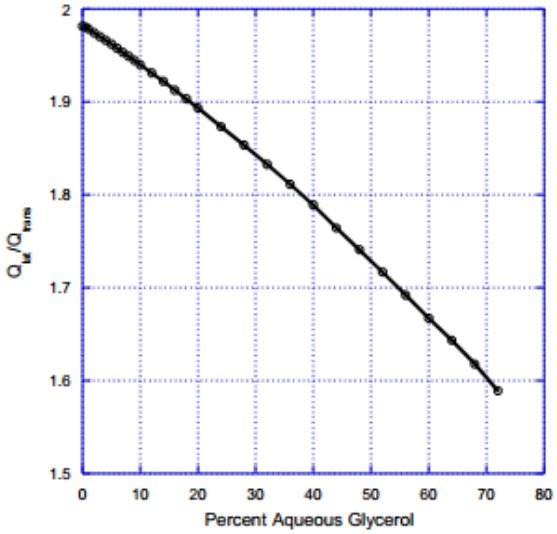

Figure 4.11: The simulated ratio of the quality factors of a laterally and a transversely vibrating beam for our 80x4x2µm resonant sensor as a function of percent aqueous glycerol in the operational medium.

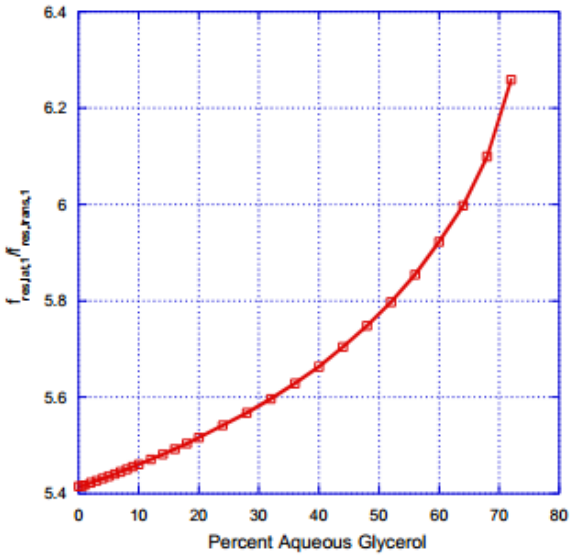

Figure 4.12: The simulated ratio of the fundamental resonant frequency of our 80x4x2µm resonant sensor vibrating laterally to the resonant frequency of the same microcantilever vibrating transversely as a function of percent aqueous glycerol found in the operational medium

Based on the formulae highlighted above, the table 2 shows a computational comparison of the current (out-of-plane) design and the proposed (in-plane) design. We see clearly a trend in better characteristic values.

	In Air			**In Media**		
	Sm (Hz/pg)	**Q**	***ω* (kHz)**	**Sm (Hz/pg)**	**Q**	***ω* (kHz)**
Current Design (Out-of-plane)	3.0	4.8	160	.221	1.5	60
Design 1	15.0	7.1	400	1.2	3.2	150
Design 2 (a and b)	17.2	7.3	410	1.6	3.3	180
Design 3	18.8	7.8	500	1.8	3.8	190
Design 4 (Optimal) (In –plane)	21.0	8.0	590	1.5	5.1	210

Table 4.1: Showing Mass Sensitivity values and quality factor and resonant frequencies for our various Sensor Geometries using semi-Analytical formulae.

Chapter 5

Results and Conclusions

In this chapter, plots of results generated from formulae in the last chapter are shown. The trends in characteristic of resonant sensor with dimensions, Reynolds number of media used (10 - 70% glycerol in this case) are presented.

In order to more accurately determine the advantage of using our in-plane over the current out-of-plane design for a dynamically driven resonant sensor, relevant characteristics such as the beam's resonant frequency and quality factor were obtained for similar beams excited both laterally and transversely.

The advantages of using our proposed in-plane mode resonant sensors are summarized and the optimal cantilever geometries for better sensing characteristics will be identified. A few issues including viscosity of fluid and actuation source are also discussed, after which a final design is proposed based on some optimal design parameters.

5.1 Results:

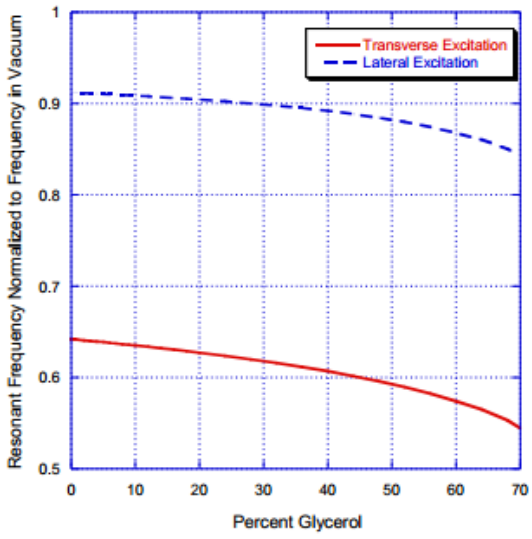

Fig 5.1: : Simulated normalized resonant frequency of a 80x4x2 um vibrating laterally and transversely in concentrations of up to 70% aqueous glycerol. Note the drastic drop in the resonant frequency for the transverse mode compared to the lateral mode.

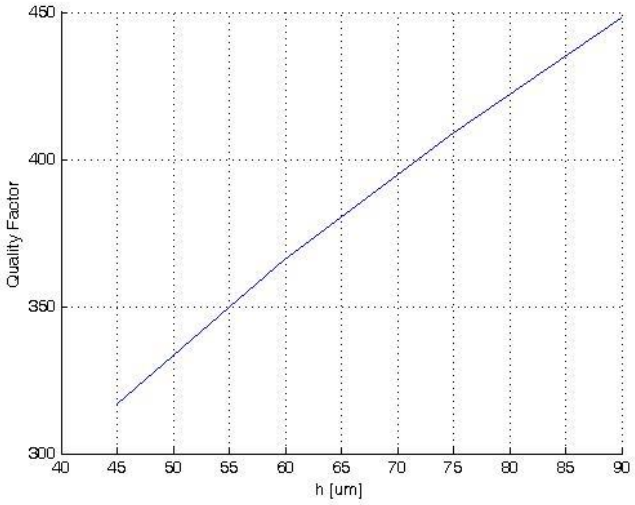

Figure 5.2: Plot of normalized Quality factor of optimal against thickness of optimal in-plane sensor showing the linear trend.

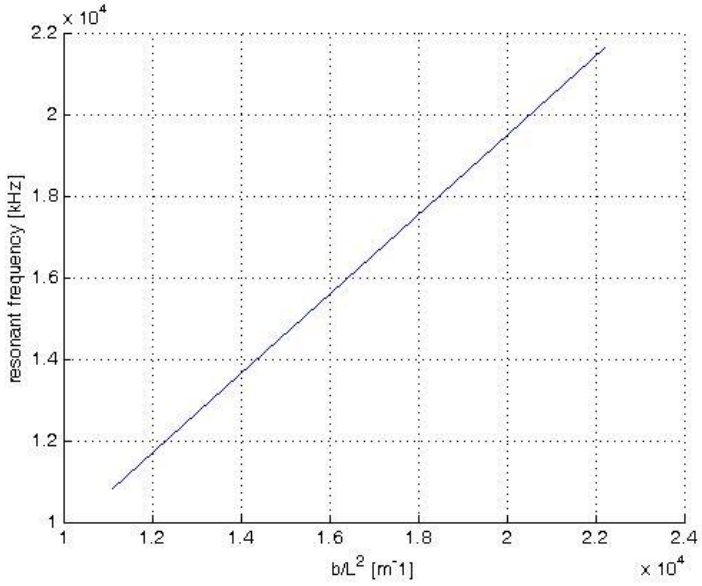

Figure 5.3: Simulated Resonant Frequency of optimal in-plane sensor against its dimension ratios

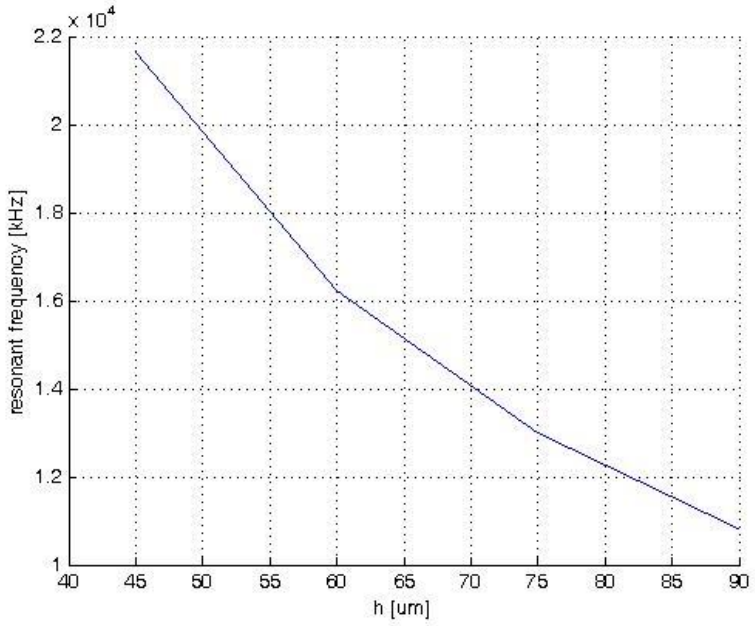

Figure 5.4: Simulated normalized Resonant Frequency against thickness of the optimal sensor. Note the drastic drop in the resonant frequency for the lateral mode

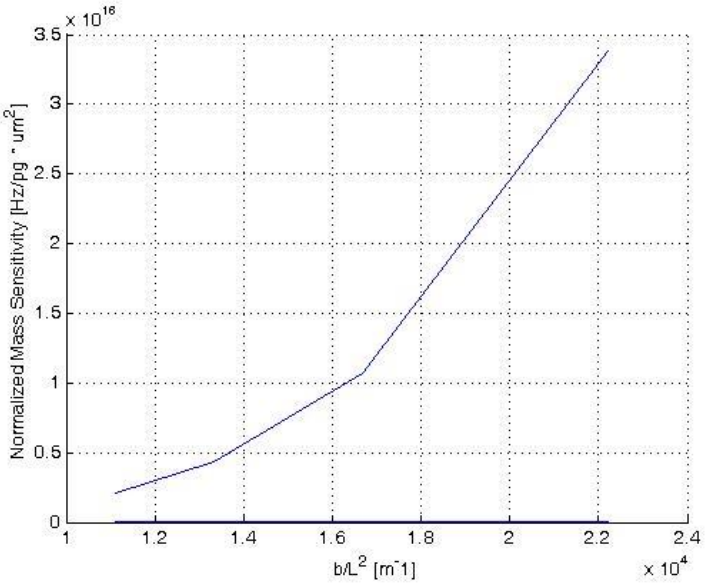

Figure 5.5: Plot of normalized mass sensitivity against thickness of 80 X 4 X 2 µm our optimal pedestal beams optimal sensor.

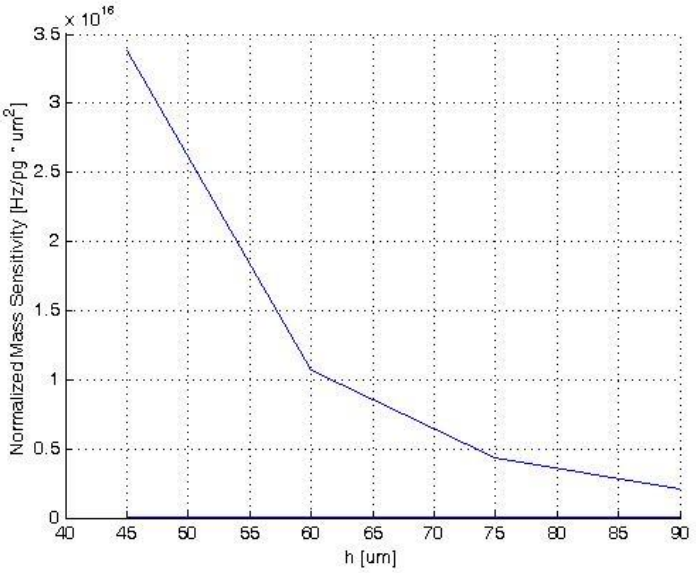

Figure 5.6: Simulated normalized mass sensitivity against thickness of 80 X 4 X 2 µm of our optimal pedestal beams optimal sensor.

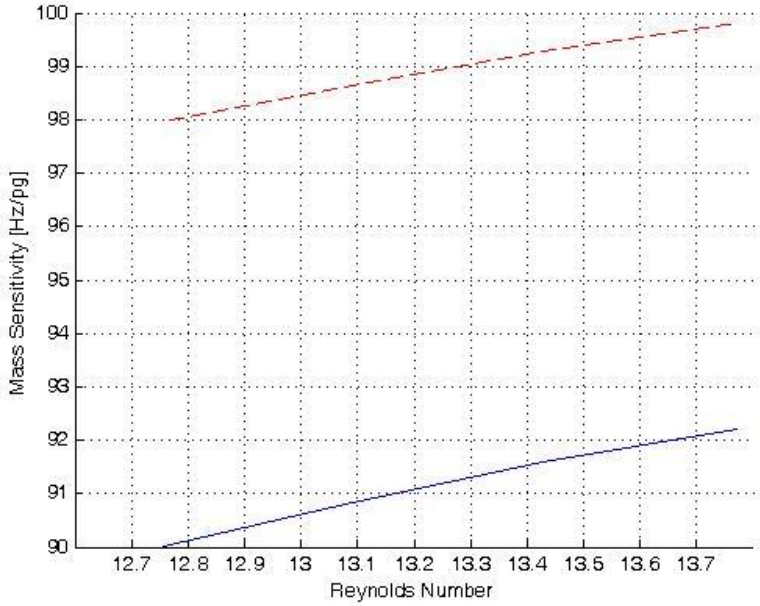

Figure 5.7: Simulated normalized Mass Sensitivity against Reynolds Number of 10% acqueous glycerol Dotted lines: lateral mode and Blue lines: Transversal mode. Beams are 80 X 4 X 2 µm

The primary objective of this work was to theoretically characterize and compare the characteristic of resonant sensors vibrating in-plane (lateral mode) and out-of-plane (transversal) direction and note the improvement when the microcantilever is excited in the in-plane direction. Dynamically driven resonant sensors are commonly vibrated in the transverse or out-of-plane direction in both gas-and liquid phase sensing applications. However, microcantilever sensors vibrating in the transverse direction have a dramatic increase in their detection limit in liquid –phase sensing applications compared to gas-phase sensing applications due to the decrease in the device's resonant frequency, quality factor and chemical sensitivity. It was expected that these characteristics would improve for beams vibrating in-plane or lateral direction due to the decreased viscous drag of beam.

Earlier experimental results given in the literature have also shown that microcantilevers have higher resonant frequencies and quality factors when operating in the in-plane flexural mode as opposed to the out-of-plane flexural mode. In order to successfully characterize laterally vibrating our proposed resonant frequency, standard Euler-Bernoulli beam theory was used to model the deflection of the beam as a function of the frequency of excitation. The deflection was found to also depend on the properties of the resonant sensor (dimensions, surface area and the configuration) and the hydrodynamic forces from the operational medium acting on the beam. The hydrodynamic forces is the sum of the pressure and shear forces. It was derived off Stokes Theorem.

In conclusion, for the design 4 chosen in chapter 4, the quality factor and mass sensitivity were found to increase when the sensor was simulated in the in-plane flexural mode compared to the out-of-plane flexural mode, with quality factors of laterally vibrating beams reaching values as high as 5.1 when operating in media.

5.2 Future Work:

The work done in this investigation can easily be expanded upon and improved. The sensing layer and area effects were not discussed elaborately in this investigation. The effects of different thickness of particular viscoelastic sensing layers on the characteristics of laterally vibrating beams can be incorporated into the model. The simulation was carried out mostly using semi-analytical and some numerical formulae. Further work will be done using Finite Element Methods tools (COMSOL or ANSYS) to show a more rigorous and numerical basis for the work done. It is believed these tools would give a better insight the characteristics obtained in this work.

Also, the actuation mechanism would be looked into. A proposed excitation source is the piezoelectric actuation source. Coupled with this is the fabrication and implementation part of the work to be done.

5.3 Reference

1) A. Jemal, R. Siegel, J. Xu, and E.Ward. Cancer Statistics, 2010. CA: A Cancer Journal for Clinicians, 60(5):277{300, 2010.
2) *Kidong Park, et.al.* Measurement of adherent cell mass and growth.
3) *Kidong Park*, et.al 'Living cantilever arrays' for characterization of mass of single live cells in fluids.
4) *Stephen M.Heinrich, et.al* A multi-modal continuous-systems model of a Novel High-Q Disk Resonator in a viscous liquid,
5) *Stephen M.Heinrich, et.al* Laterally Vibrating Symmetric Hammerhead Micro cantilevers in viscous liquids, Lateral-Mode Vibration of Micro cantilever-Based Sensors in Viscous Fluids using Timoshenko Beam Theory. *Joshua A. Schultz*
6) . *Elise Anne Corbin* Detection of Mass, Growth Rate, and Stiffness of Single Breast Cancer Cells using Micromechanical Sensors
7) Single Cell studies of the cell cycle and some models. *JM Mitchison*
8) Increased Asymmetric and Multi-Daughter Cell Division in Mechanically Confined Microenvironments. *Dini Di Carlo et.al.*
9) *Gabriel Popescu*. Optical imaging of cell mass and growth dynamics.
10) *Scott. R Manalis.et.al* Using buoyant mass to measure the growth of single cells G. Y. Chen, R. J. Warmack, T. Thundat, D. P. Allison, and A. Huang. Resonance response of scanning force microscopy cantilevers. Review of Scientific Instruments, 65(8):2532–2537, 1994.
11) S. Dohn, R. Sandberg, W. Svendsen, and A. Boisen. Enhanced functionality of cantilever based mass sensors using higher modes. Applied Physics Letters, 86(23):233501, 2005.
12) K. Park and R. Bashir. MEMS-based resonant sensor with uniform mass sensitivity. 15th International Conference on Solid-State Sensors, Actuators and Microsystems.
13) *J.E. Sader.et.al* Spring constant calibration of atomic force microscope cantilevers of arbitrary shape. Center for Disease Control and Prevention/ National Center for health Statistics. 2012
14) Wolfe, Stephen L. (1972). Biology of the cell. Wadsworth Pub. Co. ISBN 978-0-534-00106-3.
15) Arpita Upadhyaya: Article on Soft Matter: Mechanical Properties of Cells. 2013
16) Moon-Taek Park and Su-Jae Lee, Journal of Biochemistry and Molecular Biology, Vol. 36, No. 1, 2003, pp. 60-65
17) Kathleen Collins, Tyler Jacks, and Nikola P. Pavletich, The cell cycle and cancer, PNAS 1997 94 (7) 2776-2778
18) A. Tzur, R. Kafri, V. S. LeBleu, G. Lahav, and M. W. Kirschner. Cell growth and size homeostasis in proliferating animal cells. Science, 325(5937):167–171, 2009.
19) H. Lodish, A. Berk, P. Matsudaira, C. A. Kaiser, M. Krieger, M. P. Scott, L. Zipursky, and J. Darnell, *Molecular Cell Biology*, Fifth. Macmillan, 2004, p. 17.
20) W.R. Hogg, W. Coulter; Apparatus and method for measuring a dividing particle size of a particulate system; United States Patent 3557352
21) A. Tzur, R. Kafri, V. S. LeBleu, G. Lahav, and M. W. Kirschner. Cell growth and size homeostasis in proliferating animal cells. Science, 325(5937):167{171, 2009.
22) D. D. Carlo and L. P. Lee. Dynamic single-cell analysis for quantitative biology. Analytical Chemistry, 78(23):7918{7925, 2006.

23) Gere, J. M. and Timoshenko, S. P., 1997, Mechanics of Materials, PWS Publishing Company.
24) R. Cox, F. Josse, S. Heinrich, I. Dufour, O. Brand, Resonant microcantilevers vibrating laterally in viscous liquid media
25) R. Cox, F. Josse, S. Heinrich, I. Dufour, O. Brand, Damping and mass sensitivity of laterally vibrating resonant microcantilevers in viscous liquid media
26) Brumley, D., Willcox, M., and Sader, J., "Oscillation of Cylinders of Rectangular Cross section Immersed in Fluid" Physics of Fluids, vol. 22, no. 052001, 2010
27) Heinrich, S. M., Maharjan, R., Beardslee, L. Brand, O., Dufour, I., and Josse, F. "An analytical model for in-plane flexural vibrations of thin cantilever-based sensors in viscous fluids: applications to chemical sensing in liquids," Proceedings, International Workshop on Nanomechanical Cantilever Sensors, Banff, Canada, pp. 2, 2010
28) Heinrich, S. M., Maharjan, R., Dufour, I. Josse, F., Beardslee, L. and Brand, O. "An analytical model of a thermally excited microcantilever vibrating laterally in a viscous fluid," Proceedings IEEE Sensors 2010 Conference, Waikoloa, Hawaii, pp. 1399-1404., 2010
29) Kanwal, R. P., "Vibration of an Elliptic Cylinder and Flat Plate in a Viscous Fluid" Journal of Applied Mathematics and Mechanics, vol. 35, iss. 1-2, pp. 17–22, 1955
30) R. Cox, F. Josse, S. Heinrich, I. Dufour, O. Brand, Resonant Microcantilevers Vibrating Laterally in Viscous Liquid Media
31) D. M. Gryte, M. D. Ward, and W. S. Hu, "Real-time measurement of anchorage-dependent cell adhesion using a quartz crystal microbalance.," *Biotechnol. Prog.*, vol. 9, no. 1, pp. 105–8, 1993.
32) M. Mir, Z. Wang, Z. Shen, M. Bednarz, R. Bashir, I. Golding, S. G. Prasanth, and G. Popescu, "Optical measurement of cycle-dependent cell growth.," *Proc. Natl. Acad. Sci. U. S. A.*, vol. 108, no. 32, pp. 13124–9, Aug. 2011.